Synthesis and characterization of ODS-304L steels by mechanical alloying

A thesis submitted in partial fulfilment of the
requirements for the degree of

Master of technology

in

Mechanical engineering

[Specialisation: Steel technology]

by

Sandeep E S
(Roll no: 212mm2459)

Department of metallurgical and materials engineering
National institute of technology Rourkela
Rourkela, Orissa-769008

Synthesis and characterization of ODS-304L steels by mechanical alloying

A thesis submitted in partial fulfilment of the
requirements for the degree of

Master of technology

in

Mechanical engineering

[Specialisation: Steel technology]

by

Sandeep E S
(Roll no: 212mm2459)

Under the guidance
of

Prof. Swapan Kumar Karak

Department of metallurgical and materials engineering
National institute of technology Rourkela
Rourkela, Orissa-769008

National Institute of Technology Rourkela
Orissa-769008

Certificate

This is to certify that the thesis entitled "**Synthesis and characterization of ODS-304L steels by mechanical alloying**", submitted to the National Institute of Technology, Rourkela by **Mr Sandeep E S**, Roll No: **212MM2459** for the award of Master of Technology in Mechanical Engineering, at the National Institute of Technology, Rourkela, is an authentic work carried out by him under supervision and guidance. The experimental work and analysis of results are original work of the student and have not been presented anywhere for the award of a degree to the best of our knowledge.

Date:

Prof. Swapan Kumar Karak
Dept. of Metallurgical and Materials Engineering
National Institute of Technology
Rourkela- 769008

National Institute of Technology Rourkela
Orissa-769008

Declaration

I certify that

a) The work contained in the thesis is original and has been done by myself under the general supervision of my supervisor.
b) The work has not been submitted to any other Institute for any degree or diploma.
c) I have followed the guidelines provided by the Institute in writing the thesis.
d) Whenever I have used materials (experimental analysis, and text) from other sources, I have given due credit to them by citing them in the text of the thesis and giving their details in the references.
e) Whenever I have quoted written materials from other sources, I have put them under quotation marks and given due credit to the sources by citing them and giving required details in the references.

Date: Sandeep E S

Acknowledgement

With deep regards and profound respect, I avail this opportunity to express my deep sense of gratitude and indebtedness to **Prof. Swapan Kumar Karak, Department of Metallurgical and Materials Engineering, NIT Rourkela**, for introducing the present research topic and for his inspiring guidance, constructive criticism and valuable suggestion throughout this research work. It would have not been possible for me to bring out this report without his help and constant encouragement.

I express my sincere gratefulness to Dr. B C Ray, Head of the Department, Metallurgical and Materials Engineering, NIT Rourkela for giving me an opportunity to work on this project and allowing me the access to valuable facilities in the department.

I am very much thankful to Dr. B Mishra, Deputy Director of DISIR for allowing me the access to valuable facilities in their research centre.

My special thanks go to Prof. D Chaira, Prof. A Basu, Prof. A Malik for providing facility and giving me the valuable suggestion to carry out this project and also all professors of this department. I am highly grateful to laboratory members of the Department of Metallurgical and Materials Engineering, NIT Rourkela, especially, Mr. U.K. Sahu, Mr. Pradhan, Mr. A. Pal, and Mr. Kishore Tanty for their help during the execution of experiments.

Last but not the least I would like to thank Mohan N, Sravan S and Shashanka R, all my classmates and my dear friends especially Lenin, Arjun, Suvin and Anil for their encouragement and understanding. Most importantly, none of this would have been possible without the love and patience of my family. My family, to whom this dissertation is dedicated, has been a constant source of love, concern, support and strength all these years. I would like to express my heart-felt gratitude to them.

Sandeep E S
sandeepsajeevan049@gmail.com

Abstract

Nano-oxide dispersed austenitic stainless steels are extensively used in nuclear industry, high performance pressure vessels, chemical and medical industry due to their superior mechanical properties, good weight to strength ratio, durability and very good corrosion resistance.Strength of the ODS alloys could be appreciably enhanced by uniform dispersion of higher amount of nanometric Y_2O_3 and TiO_2.

The present study aims at synthesis of 70.00Fe-19.00Cr-11.00Ni (alloy A), 69.00Fe-19.00Cr-11.00Ni with 1.0 % Y_2O_3dispersed (alloy B) and 69.00Fe-19.00Cr-11.00Ni with 1.0 % TiO_2 dispersed (alloy C) all in wt. %, through mechanical alloying followed by conventional sintering. Sintering of the alloy powders (alloy A, alloy B and alloy C) are carried out in argon atmosphere at 1150°C for 1.0 hour. Characterization has been undertaken in different stages of milling like 1h, 5h, 10h, 15h, 20h, 30h and 40h of mechanical alloyed powders and sintered pellets, by X-ray diffraction study (XRD), scanning electron microscopy (SEM) and energy dispersive spectroscopy (EDS). The XRD peaks of powder gradually get broadened with increase in milling time. Particle size of milled powders have been measured by using particle size analyser and find the average particle size get reduced from 51.2 µm to 7.5µm with increasing milling time. Physical (density and porosity) and mechanical (hardness and wear resistance) properties of the sintered pellets were evaluated. The density of sintered products has been calculated by using Archimedes principle. The sintered density of alloy C (1.0 wt. % TiO_2 dispersed) is the best as compared to that of alloy A and alloy B.

Vickers microhardness value is highest for alloy C (1.0 wt. % TiO_2) (4.217GPa) as compared to that of alloy A (2.628 GPa) and alloy B (1.0 % Y_2O_3) (4.033 GPa). Similar kind of trend is found in wear resistance property of the sintered pellets. Hence, it can be summarised that oxide dispersions yield at least 1.5 times greater hardness than that of base alloy.

Keywords: Mechanical alloying, Oxide dispersed austenitic steels, conventional sintering, density, XRD, SEM, mechanical properties.

Contents

List of Figures

List of Tables

1. Introduction

1.1 Background

Nuclear energy has been widely accepted as the ever increasing world energy needs. Among nuclear reactors generation IV reactors are the latest technology which has better energy utilization, improved reliability, better reactor life, improved explosion resistance and safety makes it superior from others. Nuclear power plants demands highest safety standards which led to the usage of stainless steel as it helps preventing the failure due to corrosion. Austenitic stainless steels are extensively used in nuclear industry, high performance pressure vessels, chemical and medical industry due to their superior mechanical properties, good weight to strength ratio, durability and very good corrosion resistance [1]. Austenitic stainless steel 304L is a good choice for structural components of pressurized water reactors such as reactor vessels and piping systems in comparison with ferritic steel due to its already proven superior corrosion resistance and much available data on its actual industrial use [2,3]. To improve mechanical properties of steels at high temperature, dispersion strengthening by oxide particles is done by mechanical alloying. Core components and Structural materials of nuclear reactors require better swelling characteristics, but austenitic stainless steels shows poor swelling resistance. Oxide dispersed strengthened (ODS) austenitic steels have the ability to suppress void formation due to slow recovery of initial dislocation structure immobilized by oxide particles [4]. Oxide dispersed strengthened Fe based alloys are the only materials showing high dimensional stability and high temperature strength properties resulting from the homogenous dispersion of oxide particles into metal matrix [5].

Even though austenitic stainless steels are having good creep and excellent corrosion resistance at high temperature, its high temperature strength is less when compared to other steels which are used in nuclear industry [6, 7]. It has been illustrated that in ODS ferritic steels by introducing oxide particles is one of the effective way to increase high temperature strength [8, 9]. To enhance the mechanical properties of 304L austenitic stainless steel an attempt has been made to develop Y_2O_3/TiO_2 dispersed 304L ODS steel.

1.2 Objectives

The specific objectives are:

(1) Synthesis of three different austenitic alloys with nominal compositions of 70Fe-19Cr-11Ni (alloy A), 69Fe-19 Cr-11Ni-1.0Y_2O_3 (alloy B) and 69Fe-19Cr-11Ni-1.0TiO_2 (alloy C) (all in wt. %) by mechanical alloying and followed by conventional sintering at 1150°C for 1.0 hour.

(2) Study of particle size of mechanical alloyed powder samples at different stages of milling (0h, 1h, 5h, 10h, 15h, 20h, 30h and 40 h) through particle size analysis and micro structure analysis (SEM).

(3) Study of phase evolution, microstructural evolution and chemical composition analysis in mechanical milled powder samples and sintered pellets through X-ray diffraction analysis (XRD), scanning electron microscopy (SEM) and electron dispersive spectroscopy (EDS) respectively.

(4) Evaluation and comparison of physical property (density) and mechanical properties (hardness and wear resistance) of the three different alloys.

2. Literature review

2.1 Preface

Stainless steel is an alloy of steel with minimum of 10.5 wt% chromium content in it. Stainless steel are mainly used in corrosive environments due to its excellent corrosion resistance. There are mainly three type of stainless steel based on metallurgical phases present in it, namely,

- Ferritic
- Martensitic
- Austenitic
- Duplex steels

There are various "grades" of stainless steel discrete according to their composition. Among all austenitic stainless steel are widely used in industry [10]. Austenitic stainless steels mostly consist of chromium (16-26%), nickel (6-12%), carbon (max 0.15%) and rest iron [11]. These steels are basically nonmagnetic in annealed condition, and cannot harden by heat treatment. Austenitic stainless steels are exceptionally difficult to machine and shock resistant unless they contain sulphur and selenium. Austenitic stainless steels have the best resistance to scaling and high temperature strength. Type 304 steel contains carbon content upto 0.08%. It has good weldability and decreased tendency towards carbide precipitation. To avoid carbide precipitation during welding, a lower-carbon version, type 304L steel was developed. Austenitic stainless steel possesses more corrosion resistance to both martensitic and ferritic stainless steels. Austenitic stainless steels are mainly of 200 and 300 series among all 304 grade is most widely used grade 304L grade are used in, where corrosive problems caused by welding are severe. Austenitic stainless steel have high toughness to cryogenic temperatures. They show superior thermal expansion and heat capacity with lower thermal conductivity than other stainless steels. They shows nonmagnetic nature so they can be readily welded. Other alloying elements are added to get desired properties.

Nickel and chromium contents (Wt. %) in Fe-Ni-Cr tertiary alloy determines the phases that are stable at room temperature. Fig.2.1 shows the phases stable at room temperature for corresponding weight percentages of nickel and chromium.

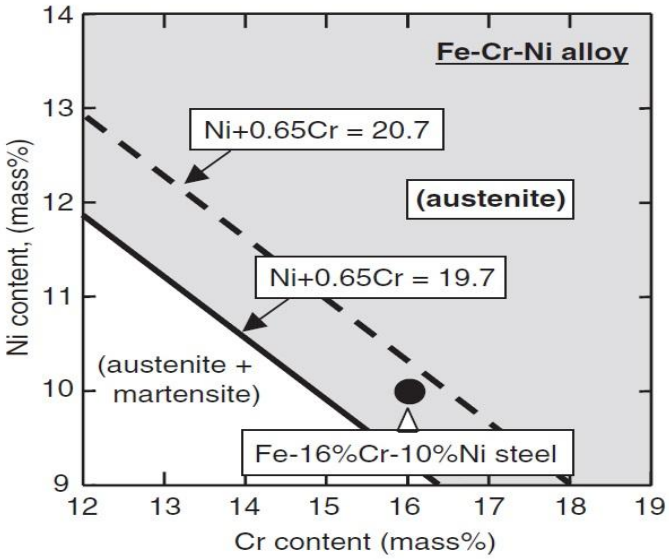

Fig. 2.1: Structure diagram at room temperature in the relation between Cr and Ni concentration for Fe-Cr-Ni ternary alloy [12].

Lines in the Fig. 2.1 express Ni equivalent to obtain fully austenitic structure at room temperature.

2.2 Fine particle strengthening mechanism

Strengthening in oxide dispersed strengthened austenitic steels is achieved by dispersoid particles acting as barriers to dislocation motion during deformation and as an increasing the load required to tear away to dislocation or bulge it through an array of particles. Strengthening depends on the interactions between particles and dislocations. Finer dispersoids have greater effect on strength than higher volume fraction [13, 14].Particles hinder dislocations and also apply a retarding force on grain boundaries that tend to migrate [15].This retarding force per unit area, F_r is given by

$$F_r = 3f\gamma_{gb} / 2r \qquad (2.1)$$

Where, f is the volume fraction of particles, r is the uniform radius of particles, and γ_{gb} is the grain boundary energy per unit area. From this equation it can be inferred that for certain volume fraction finer the particles greater will be the resistance to grain boundary movement [15].

2.3Dislocation/ particle interaction in ODS alloys.

Pinning of dislocations at hard oxide particles in an ODS alloy can be explained by several theories of the following researchers [16] such as:

a. Orowan bowing of dislocations between particles. This mechanism is for low temperature deformation. However it has been reported that testing at high temperature yielded slightly different results from the Orowan stress for ODS alloys.

b. Another mechanism **'**dislocation smearing**'**, explains the interactions between dislocations and disjointed dispersoids at elevated temperatures. The dislocation glides up to the particle and moves out over the interface between disjointed particle and matrix. This mechanism relays on diffusive processes and therefore is not likely to function at low temperatures

c. Cross slip becomes less likely to occur when there is decrease in stacking –fault energy. Since Chromium additions decrease the stacking-fault energy in Ni-Cr alloys, cross slip is expected to be unlikely in alloys with high Cr concentrations.

d. Climb over dislocations happens only if there is an attractive force between particles and dislocations. At High temperatures dislocations overcome the oxide particles by thermally activated climb, while at low temperatures where diffusion is slow, dislocation by-pass is assumed to occur by Orowan looping [17]

e. Shearing of particle can take place if a dislocation bows around a particle (soft one), there is possibility for the particle to be sheared.

2.4 Factors affecting mechanical property during strengthening

The final mechanical property of the alloy depends both on matrix and Oxide particle strengthening.

2.4.1 Matrix strengthening

The yield strength can be increased by reducing the grain size of the metallic particles. The grain size of the material can be related to yield strength hall-petch equation.

$$\sigma_o = \sigma_i + k\, d^{-1/2} \qquad (2.2)$$

where, σ_i is the "lattice friction stress" which is temperature dependent, k is the hall-petch constant, and d is the grain size of the material. K is independent on temperature, composition. As the temperature increases, dislocation recovery processes occur and Hall-petch effect becomes less effective. This happens because Hall-petch effect is based on dislocation mechanism. Subsequently weaker deformation mechanism may start to regulate the strength. In fine grained material this results in drop of yield strength at high temperatures [18]. Hence it is desirable to work with materials that possess a stable grain size at high temperatures.

2.4.2 Dispersion Strengthening:

The strengthening from dispersoids comes from the need to move the dislocations pass the particles. According to Orowan model (Orowan 1946) the resolved shear stress(τ_s) required for dislocation by-pass is given by the equation

$$\tau_s = K\,(G\,b/\lambda) \tag{2.3}$$

Where, G is shear modulus of the matrix, b is the magnitude Burgers vector of the dislocation, $\lambda$is the inter-particle spacing and K is a numerical constant [19]. To establish a relation between hardness and grain size, if hardness H is assumed to be proportional to the yield strength, it follows that

$$H = H_m + k\,d^{-1/2} \tag{2.4}$$

where, H_m-hardness of the matrix and k-Constant. From these equations it is clear that for a fixed volume fraction of dispersed particles, the hardness increases with decreasing particle diameter and for a fixed particle size, hardness increases with volume fraction of dispersoids. Therefore, strengthening is increased if the dispersoids volume fraction is high, powder particles are fine, and distribution of particles is homogeneous. High temperature stability of the particles is necessary for high temperature applications [20]. Ashby M F et al. [18] modified the Orowan model to take account of the interaction between neighbouring dislocations which had bowed the line energy of the dislocations and the inter-particle spacing. The modified model resulted in a reduction of applied stress required for by-passing to occur.

$$\tau_s = K'\,(G\,b/\lambda)\,\ln(x/2b) \approx K''\Delta\sigma_o \tag{2.5}$$

where, x is the average diameter of the circle of intersection between the particle and the slip plane,$\Delta\sigma_o$ is the increase in the tensile stress for dispersion strengthened alloys with uniform spherical particles and K''- Constant.

2.5 Development of ODS alloy

Oxide dispersion strengthened alloys (ODS) alloys are the potential structural materials for next-generation nuclear reactors which operate at temperatures much higher than present nuclear reactors. These applications demand superior alloy properties such as high creep strength and oxidation resistance.

ODS alloys contain fine second phase particles dispersed in the alloy matrix. Oxides are the best dispersoids because of their high hardness, high temperature stability, and

insolubility in the matrix. For dispersion strengthening oxides of high temperature stable reactive elements like Y, Ti, Si, Be, Al, Mg and Zr are better dipersoids than that of noble metals like Ni and Cu [21].The nature and size range of dispersed oxide particles in the alloy matrix are two key factors that decide the properties of oxide dispersion strengthened alloy.It has been reported that by increasing density of dispersoids mechanical properties such as strength (>2 GPa) and tensile ductility (40 %) are increased[8].Oxide dipersoids can be dissolved into metal matrix either by using high speed blender technique or ball milling[22].

2.6 Oxide dispersion strengthened steels

Mechanical alloying process is by far the most productive process to develop ODS alloys. ODS steels developed by this method have good high temperature properties, radiation resistance in terms of swelling and radiation embrittlement [23]. Different Oxide dispersion strengthened steels such as ODS ferritic, ODS ferritic/Martensitic (FMS) and ODS austenitic steels are being developed for applications in nuclear industry. The strengthening in ODS alloys is mainly due to fine dispersion of oxide particles which hinder the dislocation motion. Ferritic steels although having good mechanical properties, are poorer in corrosion resistance and creep properties compared to austenitic steels [24]. Also, related with ferritic-martensitic steels, austenitic steels are identified to have superior high-temperature strength and a reliable compatibility, but an inferior irradiation resistance [25]. An example of ODS ferritic steels developed for high performance is 14AlODS steels. It has yield strength of 652 MPa and Ultimate tensile strength 754 MPa which are greater than that of pre-alloyed non-ODS materials [26].

2.7 Oxide dispersion strengthened 304L austenitic stainless steel

The 304L stainless steels are the foremost integral of residual heat removal circuits of pressurized water reactors (PWR) [27]. ODS steels have excellent thermal creep resistance but poor corrosion properties limit their use in nuclear applications. To enhance the resistance to corrosion in ODS steels, different ODS austenitic steels are in developmental stage [28]. One such steel is Oxide dispersion strengthened 304L austenitic stainless steel. 304L stainless steel contains 18-20 wt. % Chromium, 8-12 wt. % Nickel and carbon content not exceeding 0.03 wt. %. ODS austenitic steels have higher values of Ultimate Tensile strength in comparison with non-ODS steels. UTS of a newly developed alloy with chemical composition Fe–18Cr–8Ni–1Mo–0.5Ti–0.35Y_2O_3 (in wt %) is approximately

1040 MPa at room temperature and 500MPa at 700^0C [29]. Compared to this conventional 304L steel has much less ultimate tensile strength value of 594 MPa [27]. In ODS steels, the substantial improvement in tensile properties even at elevated temperatures is attributed to strengthening by oxide particles. Metallic oxide particles are steady up to very high temperatures [30]. These ultrafine oxide particles (usually Y_2O_3) will slow down recrystallization, grain coarsening, and grain boundary sliding thereby significantly improving high temperature properties [31]. Addition of alloying elements such as Ti to the base composition of ODS 304L steel also induces isotropic characteristics in mechanical properties [25]. Although different strengthening mechanisms result in final mechanical properties, grain refinement and dispersion strengthening are dominant in ODS 18-8 steel [30].

2.8 Mechanical alloying

Mechanical alloying (MA) is a solid-state powder processing method involving repetitive cold welding, fracturing, and rewelding of powder particles in a high-energy ball mill. General outline of MA starts with blending powders in a required composition and mill it with a grinding medium in a high energy ball mill for desired duration of time, until the composition of milled powder particle is similar to the proportion of powder particle before milling. The milled powder is then compacted into a required shape and sintered to obtain the preferred properties and microstructure.

Suryanarayana et al. [32] Processing advanced materials under non-equilibrium conditions can control the structure and constitution of the material in a better way, which makes them to give precise properties for demanding applications. Commercially used processes to develop advanced materials include rapid solidification from liquid state, mechanical alloying, plasma processing and vapour deposition. The principle of all process is to process material in a non-equilibrium state by energising and quenching (shown in Fig. 2.2), by applying dynamic forces via externally through application of pressure, melting, irradiation, storing of mechanical energy by plastic deformation.

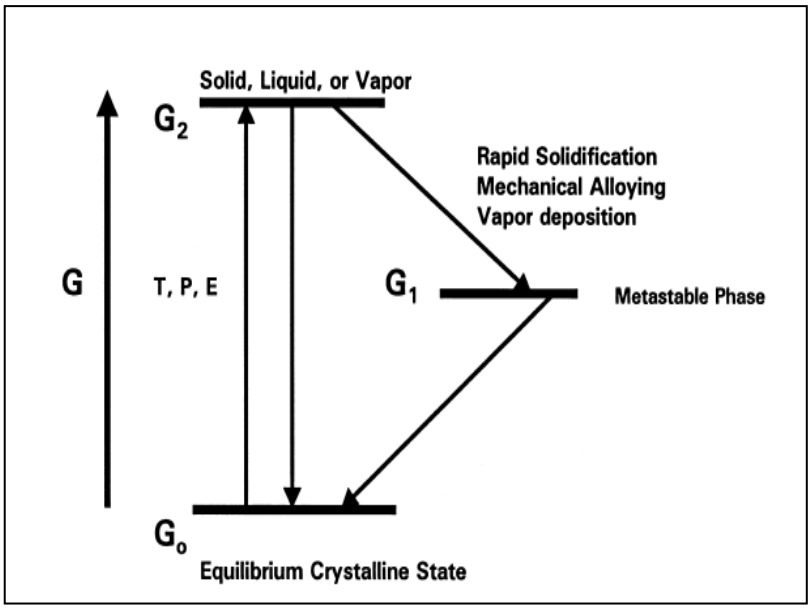

Fig. 2.2: The basic theory of "energize and quench" to produce non-equilibrium materials [32].

The deciding factor for select a process to synthesis meta-stable structure is its maximum departure from equilibrium. Table2.1summarize the departures calculated for the different processing techniques.

Table 2.1: Departure from equilibrium achieved in different non-equilibrium processing techniques [32].

Technique	**Maximum departure from equilibrium (kJ/mol)**
Solid state quench	16
Rapid solidification	24
Mechanical alloying	30
Mechanical cold work	1
Irradiation/ion implantation	30
Condensation from vapour	160

The important modules of the mechanical alloying process are raw materials, mill, and process variables. Raw materials used for mechanical alloying are commercially available powders of metals, master alloys, pre alloyed powders and refractory compounds. These powders have particle size in the range 1-200µm. The milling process is further referred as wet grinding or dry grinding depending upon whether a liquid medium is used or not [33-34]. To obtain finer particle size wet grinding is preferred over dry grinding as the solvent

molecules in wet grinding are adsorbed on the powder particle which results in lowering their surface energy [35]. Although wet grinding is advantageous in effective reduction of particle size, the major drawback is the contamination of the powder. Hence most mechanical alloying and mechanical milling processes have been carried out dry [32].

Different types of mills are used for mechanical alloying such as SPEX mills, planetary ball mills, attritor mills, Commercial mills etc., of these, planetary ball mill is one of the popular mill used for mechanical alloying. In a planetary ball mill few hundred grams can be milled at a time. Vials in a planetary ball mill are organised on a rotating support disk and a drive mechanism causes them to rotate around their own axes. The centrifugal force produced by the vials rotating around their own axes and that created by the rotation of support disk both contribute to vial constituents, consisting of material to be milled and the grinding balls [32]. Grinding vials and balls are accessible in different materials such as agate, silicon nitride, sintered corundum, zirconia, chrome steel, Cr-Ni steel, tungsten carbide, and plastic polyamide.

2.8.1 Process variables during mechanical alloying

Mechanical alloying being a complex process, involves many process variables such as:

- Type of mill,
- Milling container,
- Milling speed,
- Milling time,
- Type, size, and size distribution of the grinding medium,
- Ball-to-powder weight ratio,
- Extent of filling the vial,
- Milling atmosphere,
- Process control agent, and
- Temperature of milling.

Optimization of these variables is necessary to achieve desired microstructure, properties of the powder. More importantly the interdependence between the process variables is to be considered while optimization.

2.8.2 Mechanism of mechanical alloying

High-energy milling of powder particles involves repeated flattened, cold Welded, fractured and rewelded. During the milling process steel balls collide with each other trapping the powder particles between them shown in Fig. 2.3. Force of impact plastically deforms powder particles leading to work hardening and fracture. The new surface formed weld together and particles size increases. A broad range of particle sizes develops, with some as large as three times bigger than the starting particles. Upon continuing deformation particles get further work hardened and fatigue fracture takes place. The Fracture fragments reduce in size if there is no strong agglomeration force. Fracture tendency predominates over cold welding and due to continued impact of grinding balls the structure of the particles is steadily refined keeping their size same [32]. Milling process has very low efficiency. Even a high-energy ball milling has less than one percent efficient. Energy is lost mostly in the form of heat, utilising a small amount for particle deformation.

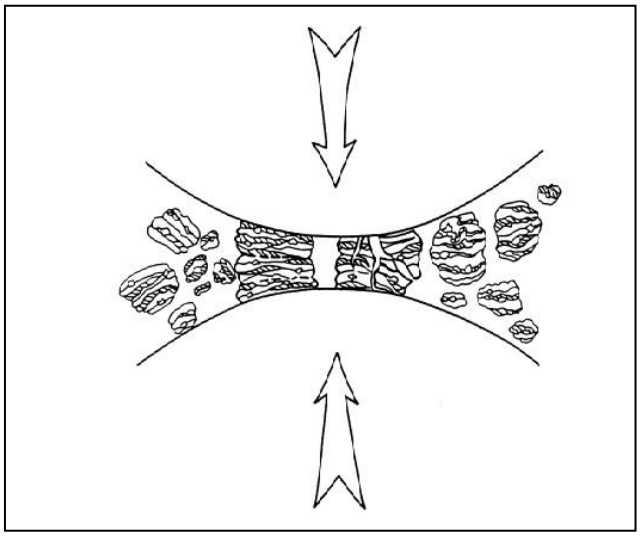

Fig. 2.3: Ball-powder-ball collision of powder mixture during mechanical alloying [32].

There are three categories of mechanical alloying with different combinations of metals and alloys:

1. Ductile-Ductile system.

The ideal combination of metals and alloys for mechanical alloying are ductile-ductile system. For the ductile-ductile combination at least 15% of ductile component are necessary for achieving mechanical alloying, because true alloying occurs due to the

repeated action of cold welding and fracturing of powder particles, which means, cold welding can occur if and only if the particles are ductile [36]. It was reported that in the initial stages of MA, the ductile components get into platelet/pancake shapes by a micro-forging process [37]. A small quantity of the powder also gets welded onto the ball surfaces which are advantageous for grinding medium, because the coating restricts further wear of it and more over contamination caused by the wear get reduced by this. But, the thickness of the powder layer must be kept to a minimum on the grinding medium to avoid the formation of heterogeneous product [38].In the second stage, these particles get cold welded together and forma composite lamellar structure of the constituent metals and it has been noticed that an increase in particle size has occurred during this stage. The composite powder particles get work hardened, with increasing mechanical alloying time as a result, the hardness and brittleness of the material get increased.

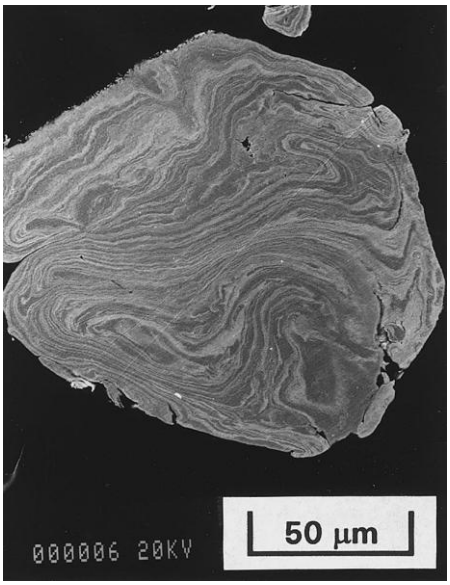

Fig. 2.4: Scanning electron micrograph showing the long-winded lamellar structure obtained during milling of a ductile-ductile component system [32].

The particles get fragmented resulting in particles with more equiaxed dimensions. With progress in milling, the coarse and fine powders and also the elemental lamellae of the welded layer become long-winded instead of being linear(Fig. 2.4).During the milling operation heat produced, decrease in inter lamellar spacing and increase in lattice defect density leads to alloying. A steady-state processing stage will attain where the hardness and particle size reach a saturation value. Formation of solid solutions, intermetallics, or amorphous phases which are the results of true alloying occurs with further milling. The layer spacing will disappears at this stage which is no longer visible under an optical microscope, which is the indication of the completion of the MA process.

2. Ductile-brittle system.

The conventional ODS alloys are under this category because the brittle oxide particles are dispersed in a ductile matrix. Benjamin and others [38, 39] described the microstructural evolution in the ductile-brittle. At the initial period of milling, the ductile metal powder particles become flattened by the force generated by the ball-powder-ball collisions, whereas the brittle oxide or intermetallic particles get fragmented. These fragmented brittle particles will trapped in the ductile particles as they tends to come in contact with the ductile constituents.

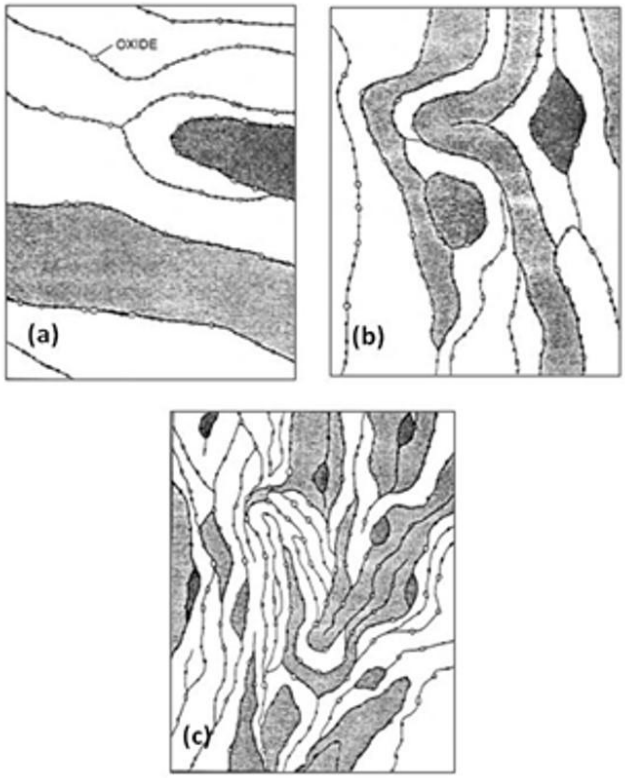

Fig. 2.5: Microstructural evolution during milling of a ductile-brittle system (ODS) [32].

In the initial stages of milling the brittle component is narrowly spaced along the interlamellar spacing (Fig. 2.5a). Through progress in milling, the ductile powder particles get work hardened causes the lamellae become convoluted, and refined (Fig. 2.5b). As a result the individual particles composition meets toward the overall composition of the starting powder mixture. Through sustained milling, the lamellae become further refined, the Inter-lamellar spacing decreases, and the brittle particles get uniformly dispersed (Fig. 2.5c). The ductile-brittle system also depends on the solid solubility of the brittle component in the ductile matrix. For mechanical alloying of ductile-brittle system, a ductile-brittle component requires both fragmentation of brittle particles to ease short-range diffusion, and also reasonable solid solubility in the ductile matrix component [40].

3. Brittle- brittle system.

An instinctive stand point suggests that alloying in a system consisting of two or more brittle components is unlikely. In absence of a ductile component it is difficult for any welding to occur, consequently alloying is also not expected to occur. There have been reports claiming that alloying occurs in brittle-brittle component systems such as Si-Ge and Mn-Bi [41, 42]. Amorphous phases were produced by milling of mixtures of brittle intermetallics [43].As mentioned above, during milling of brittle components, particles get fragmented and size reduction takes place continuously, resulting in certain size where powder particles perform in a ductile fashion. At this stage additional reduction in size of powder particles is not conceivable; this is named as the boundary of comminution [44]. While milling of brittle-brittle component systems, it can be perceived that the harder component becomes fragmented and gets embedded in the softer component. Thus Si particles which are harder are embedded in the softer Ge matrix [32].Diffusion appears to be essential for alloying to occur in all types of systems. Hence, at very low temperatures (liquid nitrogen temperatures), alloying did not happen in the brittle-brittle systems (Si-Ge) while in the ductile-ductile and ductile-brittle systems alloying occurred at sub-ambient temperatures. This may be because of the longer diffusion distances required in the brittle-brittle granular vs. ductile-ductile lamellar geometry, and/or the enhanced diffusion paths provided by severe plastic deformation in ductile-ductile systems[32].

Material transfer during milling of brittle components may be explained by mechanisms involving plastic deformation, which is resulted by (a) local temperature rise, (b) Micro deformation in defect-free volumes, (c) surface deformation, and/or (d) hydrostatic stress state in the powders during milling [42].

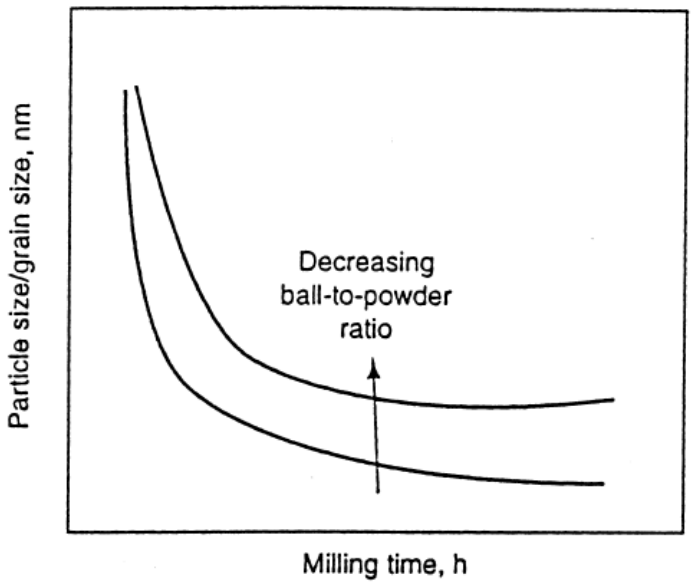

Fig. 2.6: Refinement of particle and grain sizes with milling time [32].

Rate of refinement enhances with higher milling energy, ball-to-powder weight ratio (Fig. 2.6), lower temperature etc., [32].

2.9 Powder consolidation

2.9.1. Compaction

The main purposes of metal powder compaction are:

- To compact the powder into desired shape
- To impart the preferred final dimensions with due consideration to changes resulting from sintering**.**
- To impart desired level and type of porosity [45].
- To impart adequate strength for subsequent processing.

Compaction may be done either at room temperature or at high temperature. High temperature compaction gives advantage of the modified flow behaviour of powders. Room temperature compaction hires pressures in the range of 100- 700 MPa and can provide densities in the range of 60% to 90% of the theoretical density [46].

Compaction techniques used can be differentiated by the relative movement of individual tool elements – upper punch, lower punch and die (Fig. 2.7). In general, dies are fixed and upper punch or/and lower punch are movable. If only one punch is movable it is called single action pressing. While if both the punches are movable the process is called double action pressing.

Single action pressing: -In single action pressing lower punch and die are stationary. Pressing depends solely on movement of upper punch into fixed die [45]. While pressing, pressure distribution is non-uniform in the powder due to the die wall friction.

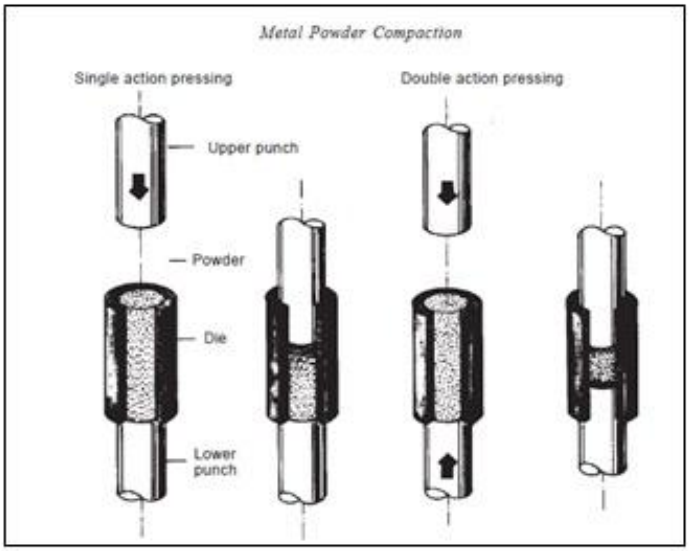

Fig.2.7: Powder compaction- Single and double acting Presses [32].

Double action pressing- In double action pressing, die is stationary but both the punches are movable. High density at the top and undersides of the compact can be attained. In the centre there remains a 'neutral zone' which is relatively weak.

2.9.2 Solid state sintering

(a) Driving forces

Elimination of internal surface area related with pores in the material is the main cause of reduction in the surface free energy during solid state sintering. Decrease in surface free energy is small when compared to other sintering processes, but the distance matter has to be transported is in the order of particle size, with the aim of occurrence of sintering at a reasonable rate and at adequately high temperature. The specific energy and curvature of particle surface provide an effective stress on the surface atoms. For a curved surface with principal radii of curvature r1 and r2, effective stress is given by young and Laplace equation [47].

$$\sigma = \gamma \mathrm{sv}\left(\frac{1}{r1} + \frac{1}{r2}\right) \tag{2.6}$$

Where γsv is the specific surface energy.

(b) Stages of sintering

There are three distinct stages in sintering. As soon as some degree of atomic mobility is achieved initial stage would begin. During this stage sharp concave necks will form between individual particles. About 5% linear shrinkage can be developed during this process. In the inter-mediate stage, high curvature formed in the first stage have been moderated and microstructure consists of three-dimensional inter penetrating network of solid particles and continuous, channel-like pores. In this stage 5-10% porosity will be persist which covers most of densification. Grain coarsening starts to become important at this stage. Grain coarsening intensity will be high during final stage [47].

(c) Mechanism of sintering

Sintering of a material can be done by several mechanisms like surface diffusion, vapour transport, lattice diffusion, grain boundary diffusion and dislocation motion. Schematic diagram of matter transport paths for two sintering particles are shown in Fig. 2.8.Vapour transport, surface diffusion and lattice diffusion from particle surfaces to the neck prime to neck growth and coarsening of the particles without densification. Grain boundary diffusion and lattice diffusion from grain boundary to the neck are the most important densifying mechanisms. Neck growth and densification through deformation of particles are caused by plastic flow by dislocation motion which is more common in metal powder sintering [47].

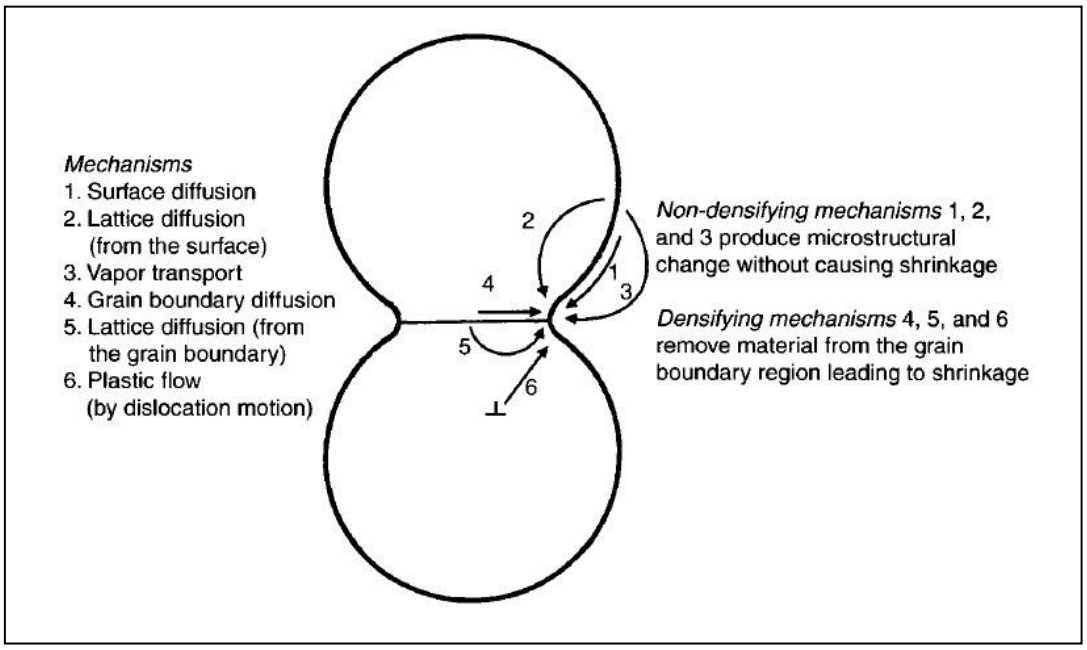

Fig. 2.8: Schematic representation of the sintering mechanisms for a system of two particles [48].

2.10 Hardness test of materials

Strength of the material can be defined by micro-hardness of the materials. Crystal structure of the material is the basis of micro-hardness property. Resistance to the localized plastic deformation offered by crystal termed as hardness. It provides mechanical property of materials like elastic constant, yield strength etc [49]. Plastic deformation of material is directly proportional to the elastic deformation developed in a material during the indentation of material. Plastic deformation and the increase in surface free energy are caused due to the absorption of energy during indentation of material.

D Taboret et al. [50]. explained different ways to measure hardness of material, namely,

- Static indentation test.
- Scratch Tests
- Plowing Tests
- Rebound Tests
- Damping Tests
- Cutting Tests
- Abrasion Test
- Erosion Tests

Micro indentation method is the most commonly used method for measuring hardness of materials. Plastic and elastic properties of indenter and indenter material are the two factors which decide hardness of material. Among static indenter tests Vickers indenter test (pyramid indenter) are found to be best for hardness measurement due to two reasons.

(a) Constant pressure for a pyramid indenter is independent of indenter size.
(b) Pyramid indenters are less affected by elastic release than other indenters.

Chapter 3: Experimental work

This chapter deals with the details of the experimental procedures carried out in this investigation. The materials were subjected to series of characterizations like X-ray diffraction (XRD), scanning electron microscopy (SEM), field emission scanning electron microscopy (FESEM), energy dispersive X-ray spectroscopy (EDS) and particle size analysis. Vickers hardness measurement and wear test has been carried out for evaluating mechanical property of the sintered alloys (alloy A, alloy B and alloy C). The details of each process are described in the following sections.

3.1 Raw materials and alloy selection

The raw materials used to prepare the desired alloys were 304L austenitic stainless steel (Fe, Cr, and Ni) pre alloyed powder and compound Y_2O_3 and TiO_2 powders. The source and purity of the powders are summarized in Table 3.1

Table 3.1: Source and purity of powders

Powder	**Source**	**Purity**
304L austenitic stainless steel	Alfa Aesar, 30 Bond street, Ward Hill, MA O1835	99.50%
TiO_2	Alfa Aesar, 30 Bond street, Ward Hill, MA O1835	99.50%
Y_2O_3	Alfa Aesar, 30 Bond street, Ward Hill, MA O1835	99.50%

The nominal composition for initial blending of the alloys synthesized in the present study is summarized in Table 3.2.

Table 3.2: Nominal composition of initial powder blends for mechanical alloying/milling.

Alloys	Fe (wt %)	Cr (wt %)	Ni (wt %)	Y_2O_3 (wt %)	TiO_2 (wt %)
alloy A	70.0	19.0	11.0	-	-
alloy B	69.0	19.0	11.0	1.0	-
alloy C	69.0	19.0	11.0	-	1.0

3.2 Synthesis of alloys by mechanical milling

Pre-alloyed 304L austenitic stainless steel powder was taken as starting material for mechanical milling. The grinding media of mechanical milling was taken as chrome steels balls and toluene as a control medium. BPR (ball powder ratio) was taken as 10:1 ratio which is 250g of grinding media and 25g of pre alloyed 304L powder. The weight of sample powder was measured using a standard weighing machine (FRITCSCH, Pulverisette-5). The weighed powder sample was added into a high energy planetary ball mill Milling has done for 40 hours with half hour cooling time for each 30 minutes of milling operation and the rotational speed has set to 300 rpm speed. To study the phases present in it and to study the changes in particle size of powder, samples were taken at an interval of 1 hr, 5hr, 10hr, 15hr, 20hr, 30hr and 40 hr respectively. The milled powder was taken out from the high energy ball mill after 40 hours of milling and kept it for drying in normal atmosphere, for the removal of toluene content in it.

3.3 Sonication and blending of alloys

To avoid agglomeration and for uniform distribution of ODS in master alloy matrix (alloy A) sonication and blending was done. 40 hours milled powder was taken from milling machine and did sonication of that sample for 1hour in a toluene bath and kept it for drying. The sonicated powder sample was divided into 3 sets, for preparing 3 different alloys. 1.0 wt % of Y_2O_3 and 1.0 wt % of TiO_2 were added to the second and third set of powder samples respectively. For getting fine dispersion mechanical blending has done for 3 hours in a blending machine and made 3 different compositions for consolidation and sintering processes.

3.4 Compaction and Sintering

The three different compositions were compacted in cold uniaxial hydraulic pressing machine at a load of 6 tonnes in a 10 mm stainless steel cylindrical die. The holding time was set to 3 minutes. For getting proper green strength of the pellets, powder weight was taken as approximately 2.4g for each consolidation process. Sintering of alloy A, alloy B and alloy C were done in a tube furnace at 1150°C for 1.0 hour in a controlled argon atmosphere. Densities of sintered pellets were measured using Archimedes' principle and tabulated in results.

3.5 Characterization of powders and sintered products

3.5.1 X-ray diffraction study (XRD)

The phase evolution of powder samples at different stages of mechanical milling and sintered pellets (alloy A, alloy B and alloy C) were studied by XRD analysis using the Cu Kα (λ=1.542Å) in a Philips X-pert MPD X-ray diffractometer. X-ray diffraction patterns were recorded from 20° to 80° scanning range with an accelerating voltage of 30 kV and at counting rate of 3°/min. The surface of the sintered samples was polished mechanically to get a straight plane on the surface before measurement to get exact peaks. XRD peaks were analysed using X' Pert High Score software for the identification of phases present in the sintered pellets.

3.5.2 Scanning electron microscopy (SEM), field emission scanning electron microscopy (FESEM) and energy dispersive X-ray spectroscopy (EDS)

Micro-structural studies of different milled powder samples and sintered pellets were studied using scanning electron microscope (SEM). EDS of milled powder sample has done for the chemical composition of each element present in it. Surface morphology of milled powders at different stages of milling has been carried out by using JEOL/EO scanning electron microscope. Surface morphology and EDS of sintered pellets were done using FESEM (NOVA NANOSEM 450)

3.6 Mechanical testing

3.6.1 Micro hardness

The micro-hardness test was executed to measure the hardness of alloy A, alloy B and alloy C using LECO (LN248AT) micro-hardness tester. The surface of the samples was mechanically polished before measurement. The micro-hardness test is more suitable for measuring the hardness of a specimen in a small scale. Experimental load applied during test was 50gf with a dwell time of 10 seconds. While loading the indenter, the indenter penetrates into the surface of the sample at constant velocity and the same velocity was applied in the unloading period, when the pyramid moved backwards. The indented area was observed and measured by a high-resolution microscope. Since the test carried in a micro scale level the hardness value was taken as the average of 10 readings. The measured hardness values were tabulated in results.

3.6.2 Study of wear behaviour

Wear resistance of the sintered samples was evaluated using a DUCOM TR-208-M1 ball on plate type wear testing instrument having a diamond indenter. The device is operated at 0.084 m/s speed and 500g load for 5 min at the ambient temperature and humidity (50-55% relative humidity).Sintered samples, subjected to wear test, were examined under optical microscope for close scrutiny of surface. Wear data obtained from the wear test and were collected and wear depth of the different alloys were plotted against time of wear.

4. Result and discussion

4.1 Phase evolution during mechanical alloying

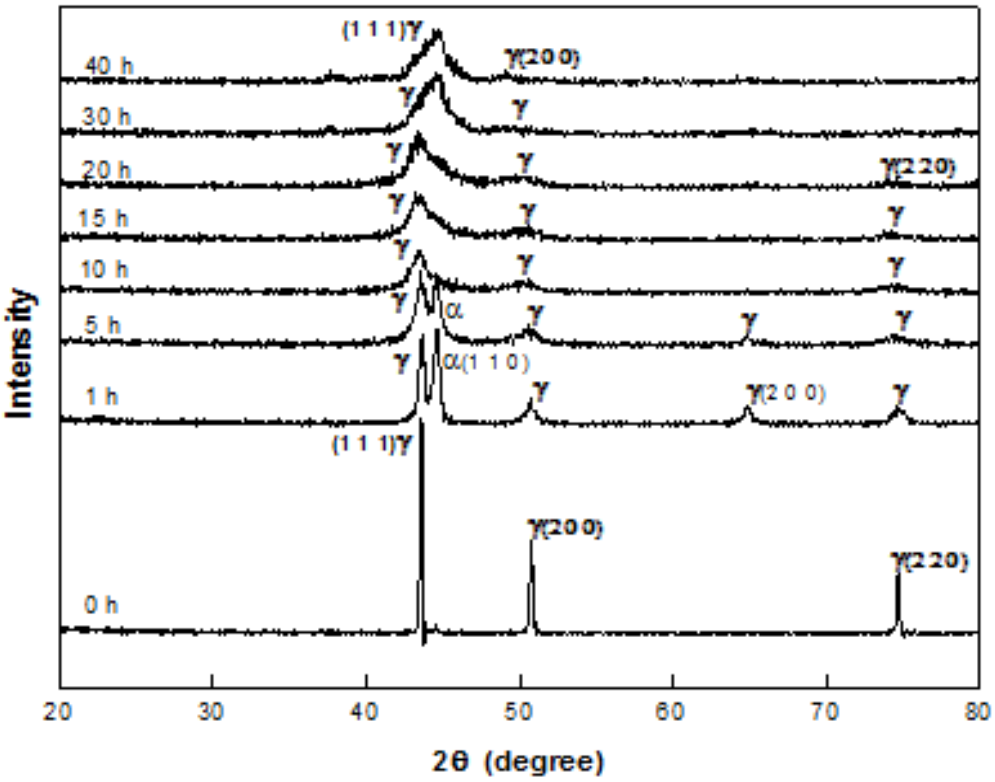

Fig. 4.1: X-ray diffraction profiles of the powder sample (alloy A) subjected to mechanical milling for 0 h to 40 h.

Fig. 4.1 shows the respective XRD patterns of the mechanically milled 304L steel powder sample (alloy A) for different increasing time periods (at 0 h, 1 h, 5 h, 10 h, 15 h, 20 h, 30 h and 40 h, respectively).From the Fig. 4.1, the milled powder (0 h) shows the high intensity peaks indicating validate presence of austenitic phase. After 1 hour of milling, Ni and Cr undergoes in solid solution of Fe matrix. The interesting phenomenon is that the new ferrite peak α and austenitic peak γ have been observed after 1 h of milling. It is observed that the austenitic peaks gradually get broaden from 5 h to 40 h of milling. It is also relevant from the peaks that number of peaks is more in initial stages of milling which shows fracturing, welding and rewelding of powder particles has happened during milling. Increase in full-width at half-maximum (FWHM) with increasing milling time depict that both plastic strain build up and crystallite size reduction are occurring.

4.2 Microstructural evolution during mechanical alloying

Fig. 4.2 (a-h) shows the microstructural features of milled powders at different stages of milling time (0h, 1h, 5h, 10h, 15h, 20h, 30h and 40h). From the Fig. 4.2 it is very clear that powders get fragmented as the milling progress. The particle size is gradually decreasing as milling time increases. The decrease in powder particle size shows that plastic strain was developed during high energy milling. After close scrutiny of the microstructural features, it is observed that the average particle size gets decreases from 50 µm to 3.5 µm.

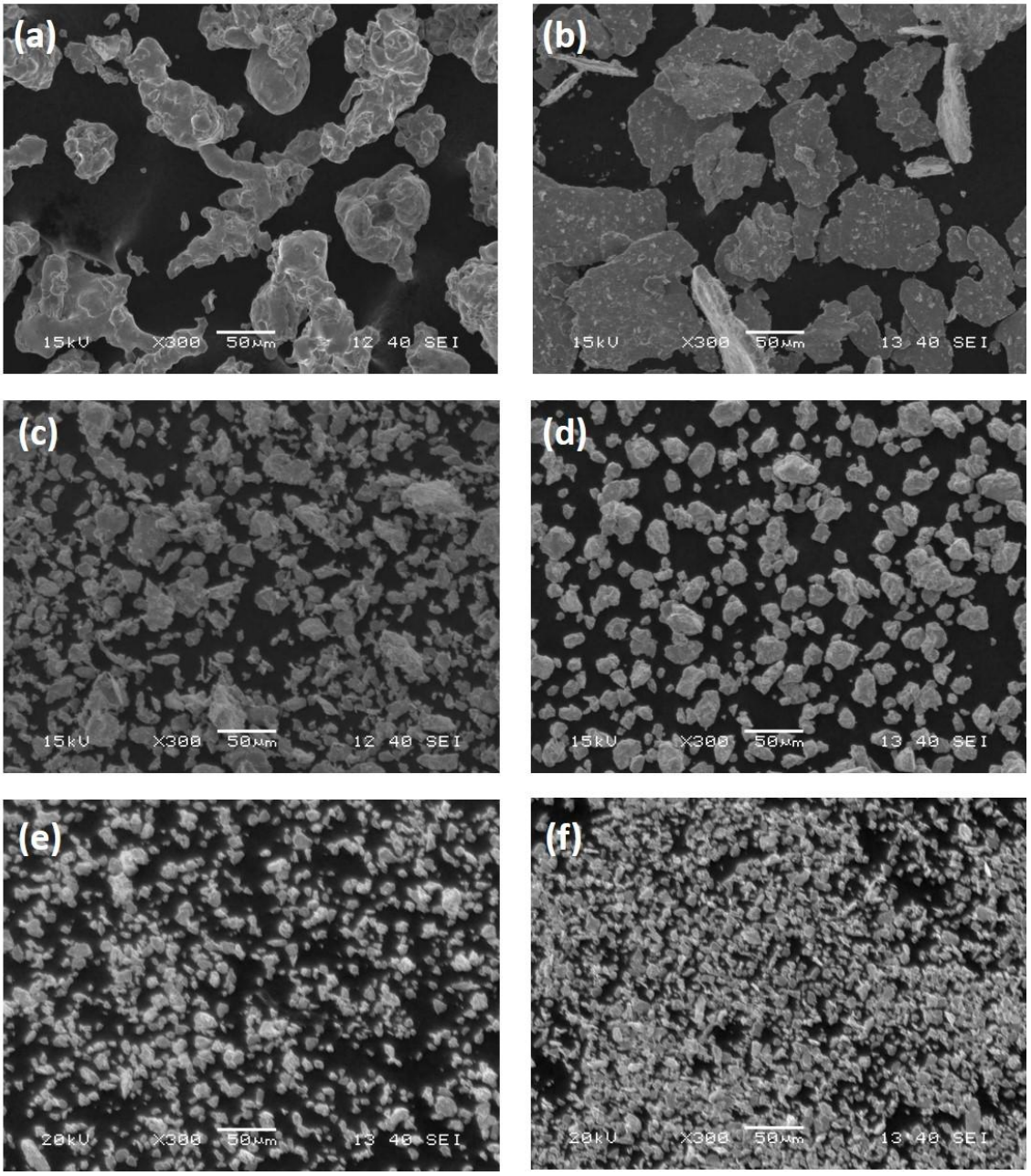

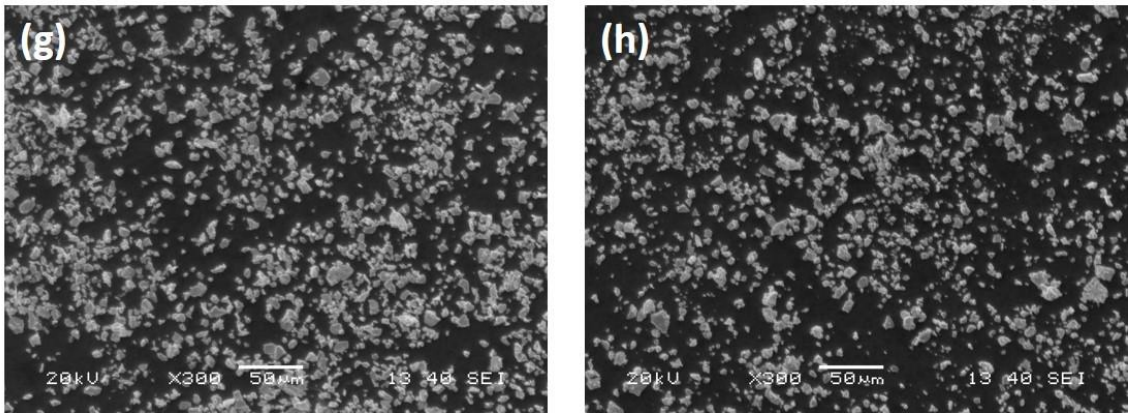

Fig. 4.2: Sem images of milled powders of alloy A: (a) 0 h, (b) 1 h, (c) 5 h,(d) 10 h, (e) 15 h, (f) 20 h,(g) 30 h and (h) 40 h.

4.3 Particle size, crystallite size and lattice strain calculation

Particle size analysis of different stages of milled powder shows the reduction of average particle size from 51µm to 15 µm with increase of milling time. The crystallite size and lattice strain is calculated by using Williamson–Hall equation [49] as follows:

$$\beta cos\theta = \left(\frac{0.94\lambda}{D}\right) + 4\eta sin\theta \qquad (4.1)$$

From the Fig. 4.3 it is clear that crystallite size decreases with the increasing milling time. It is observed that the average crystallite size gets decreases from 210 nm to 20 nm as milling time increases from 0 h to 40 h.

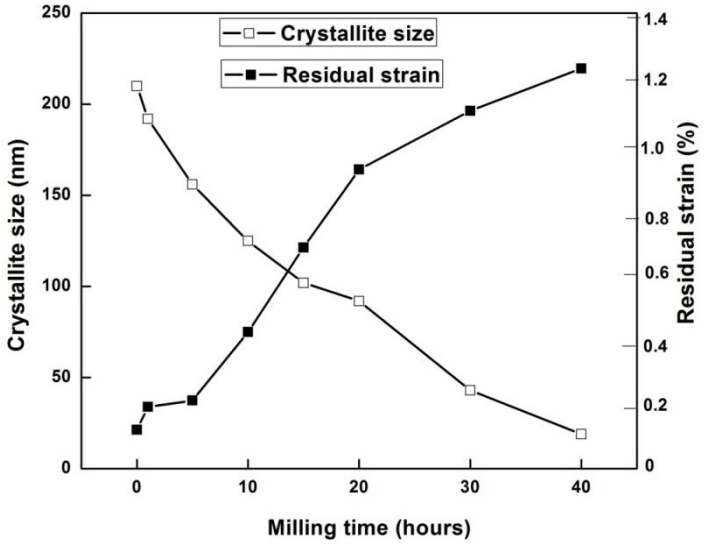

Fig. 4.3: Crystallite size and residual strain plot against milling time of milled powders (0h, 1h, 5h, 10h, 15h, 20h, 30h and 40h).

4.4 Compositional micro-analysis of alloyed powder (EDS)

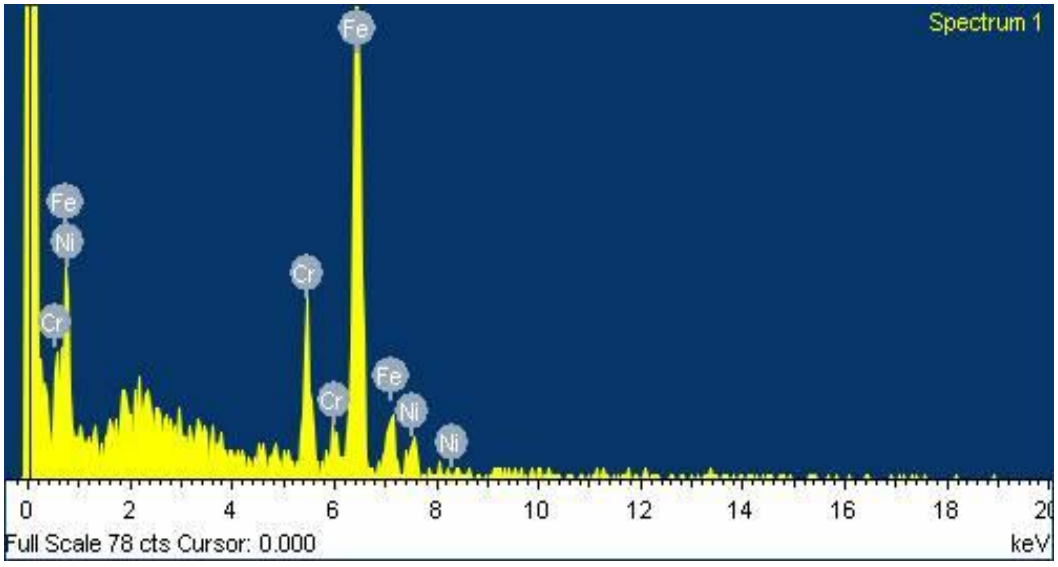

Fig. 4.4 EDS patterns of 40h milled powder of alloy A.

Fig. 4.4 shows the EDS spectrum of 40 h milled powder, revealing the presence of Fe, Cr and Ni (using quantitative EDS analysis) peaks. Table 4.1 presents the summary of EDS analysis of mechanically alloyed powder (40 h). From the table we can confirm the presence of Fe, Cr and Ni besides the results suggest that the final milled powder sustain almost same composition that present in initial powder blend. The increase in the percentage of Cr and Fe may due to the contamination from grinding medium (chrome steel balls). The changes which occurred were due to the contamination during milling which is inevitable in this condition of milling.

Table 4.1: Compositional micro analysis by EDS of 40 h milled powder of alloy A

Element	Ni	Cr	Fe
Wt.%	10.12	19.3	Balance

4.5 Phase evolution in consolidated products

Fig. 4.6 shows the XRD patterns of alloy A sintered at 1150°C for 1 hour in Ar atmosphere. It appears thatγ austenite phase is the predominant constituent and also the presence of BCC α ferrite phase has been identified in the sintered product. Similar, kind of observation have been found by Shahsanka R et al. [51].

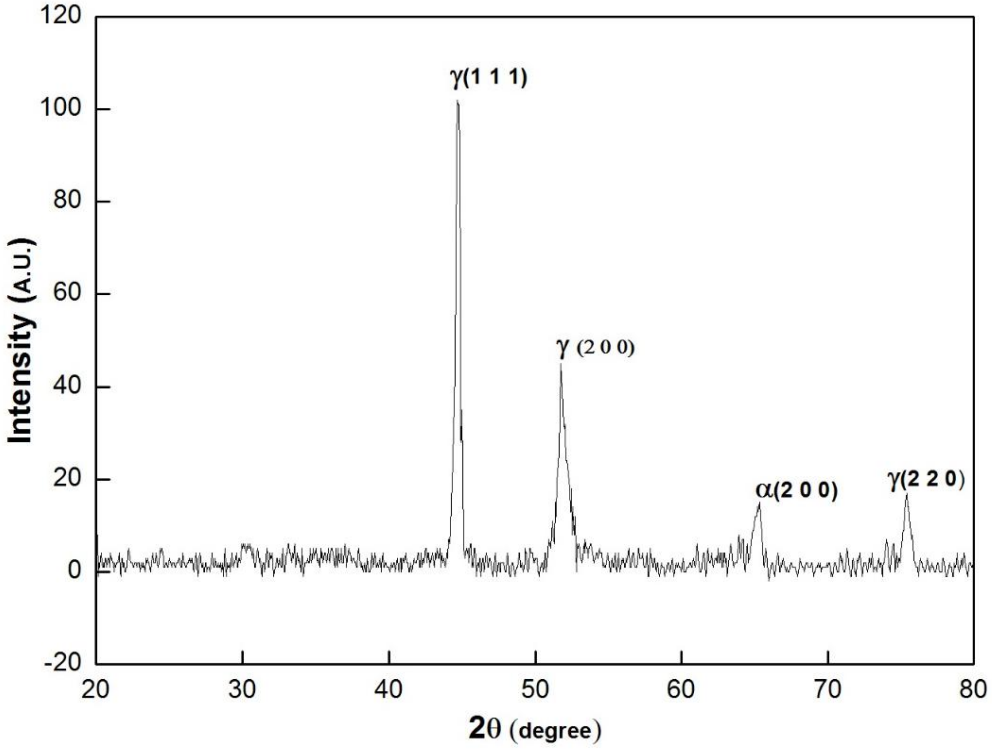

Fig. 4.5: XRD profile of sintered alloy (alloy A)

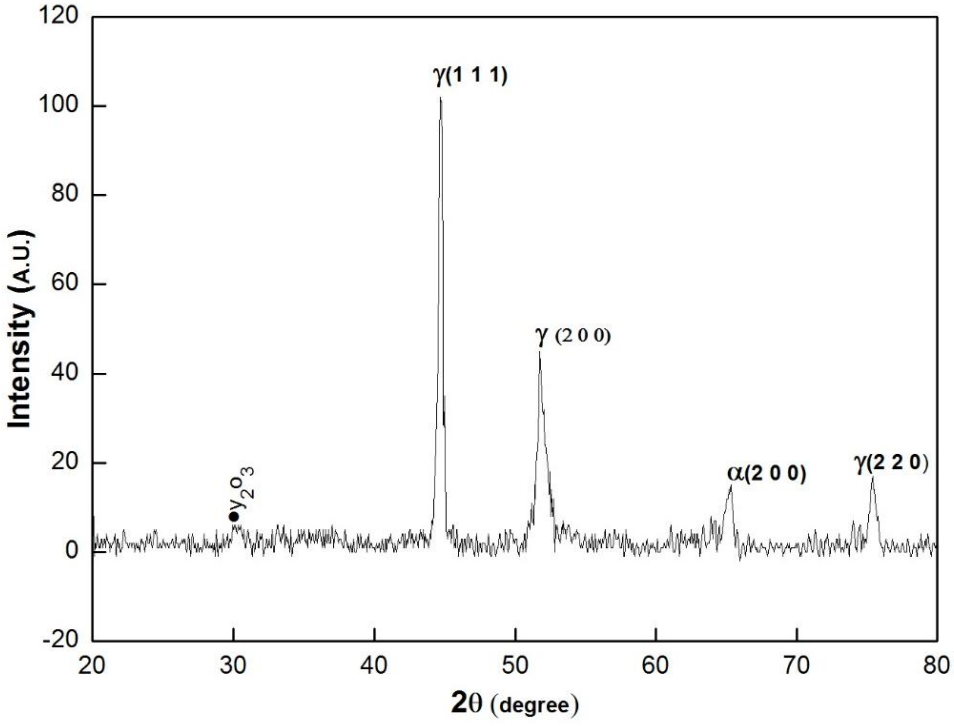

Fig. 4.6: XRD profile of sintered alloy (alloy B).

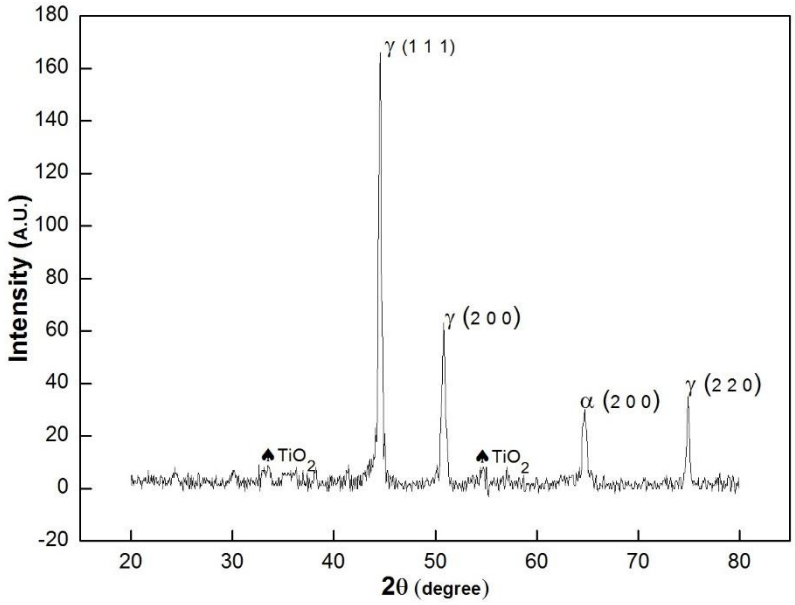

Fig. 4.7: XRD profile of sintered alloy (alloy C).

Similar kind of trends was found in the XRD profile of alloy B (Fig. 4.6) and alloy C (Fig. 4.7). In addition to the phases present in alloy A, $Y_2O_3$and TiO_2 phases were also observed in XRD profile of alloy B and alloy C, respectively.

4.6 Micro-compositional analysis of sintered alloys by EDS

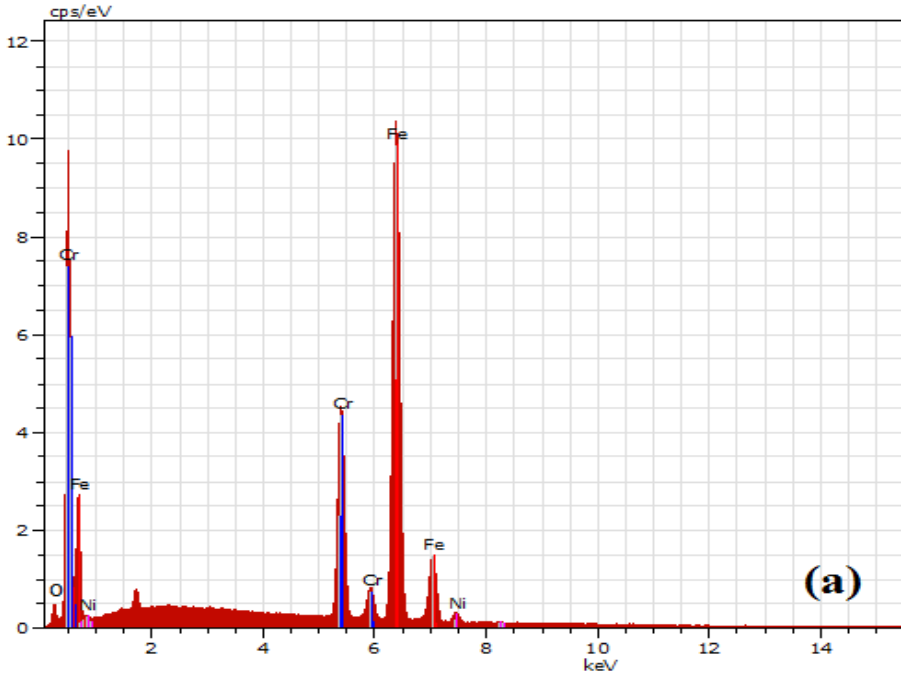

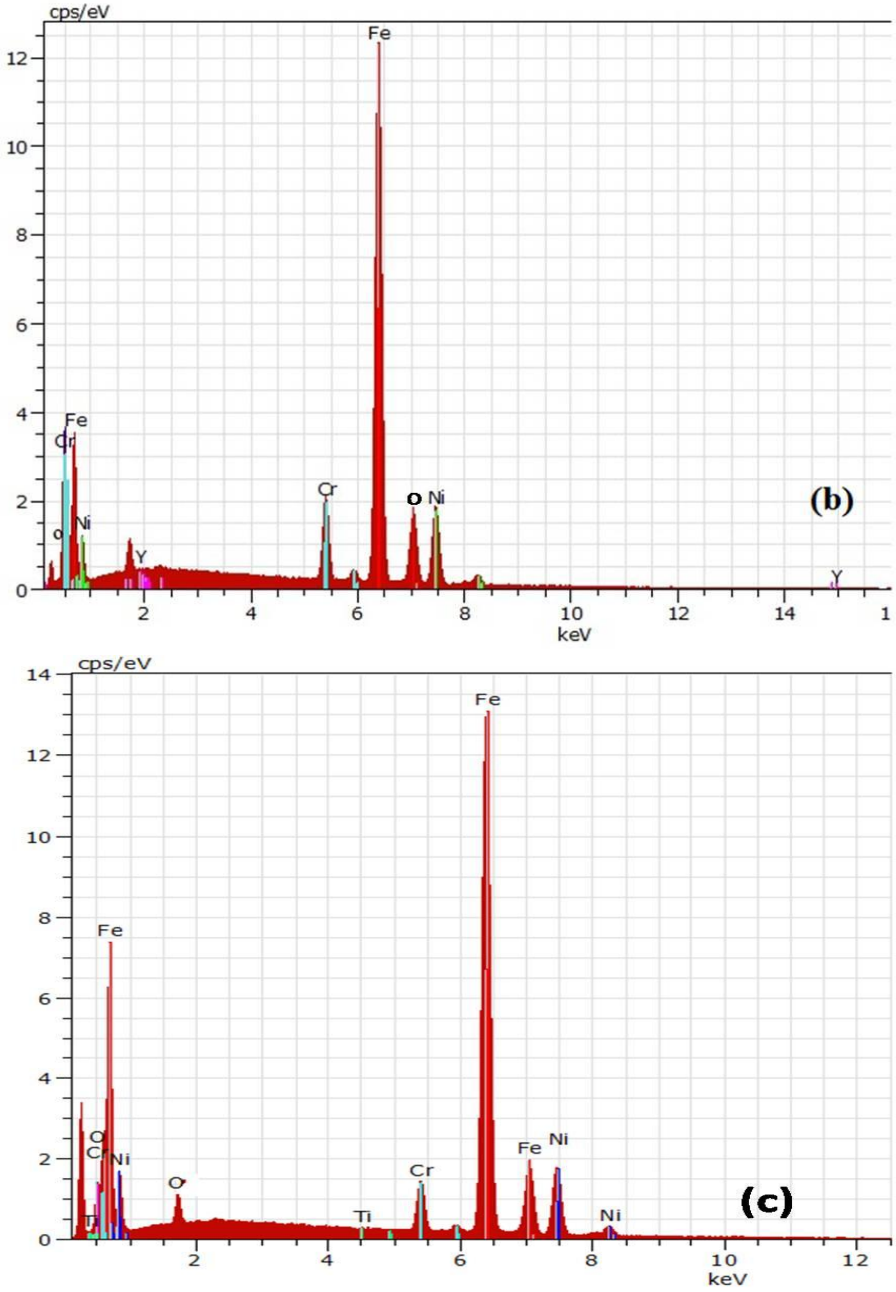

Fig. 4.8 EDS patterns of sintered pellets (a) alloy A, (b) alloy B, and (c) alloy C.

Figs. 4.8(a-c) show the EDS spectrum of all the sintered alloys, revealing the presence of predominant elements Fe, Cr and Ni. Fig. 4.8b shows the presence of predominant elements (Fe, Cr and Ni) and also element like Y and O which confirm the presence of Y_2O_3 in the austenitic matrix. Similarly, EDS spectrum of alloy C (Fig. 4.8c) confirms the presence of Ti and O which is strong evidence for the presence of TiO2 in the austenitic matrix. The micro-composition analyses from the EDS patterns (Fig. 4.8) are summarized in Table 4.2.

Table 4.2: Summary of EDS analysis of all the three alloys sintered at 1150 °C

Alloy	Elements (wt %)					
	Cr	**Ni**	**Ti**	**Y**	**O**	Fe
A	19.4	10.96	-	-	0.63	Balance
B	19.29	10.92	-	0.37	0.54	Balance
C	19.21	10.94	0.58	-	0.38	Balance

4.7 Microstructural characterization of consolidated products

4.7.1 Microstructural characterization of alloy A

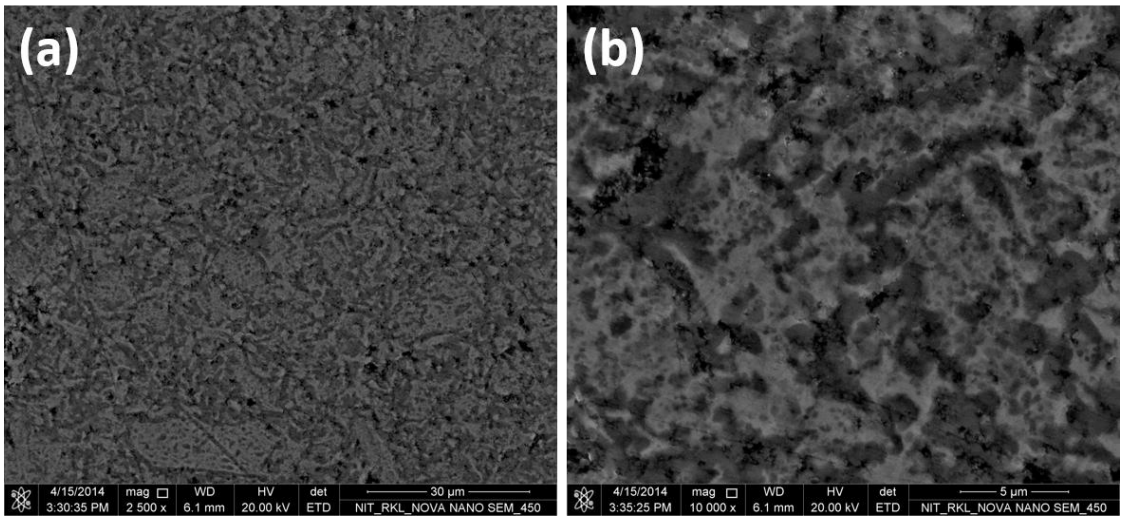

Fig. 4.9: FESEM images of alloy A at different magnifications:
(a) 2500x, and (b) 10 000x.

Figs. 4.9 (a and b) show the SEM images of the sintered pellets of alloy A at different magnifications. It reveals that the combination of bright and dark phases presence through out the microstructure. By close scruitny of the micrographs, it is clear that the bright phase belongs to ferrite and dark phase belongs toaustenite.From the EDS analysis of alloy A (fig. 4.9 (b)), the bright areas are Cr-rich (α-ferrite phase) and dark areas are Ni-rich (γ-austenite phase). The XRD results (Fig. 4.6 to 4.8) also confirm the presence ferrite and autenite phases in the sinteted pelltets. The summary of EDS analysis of bright and dark phases present in alloy A are tabulated in Table 4.3 and Table 4. 4.

Table 4.3: Summary of EDS analysis of bright phase in alloy A

Elements	Wt %
Fe	73.17
Cr	23.08
Ni	3.75

Table 4. 4: Summary of EDS analysis of dark phase in alloy A

Elements	Wt %
Fe	72.96
Ni	18.23
Cr	8.81

4.7.2 Microstructural characterization of alloy B

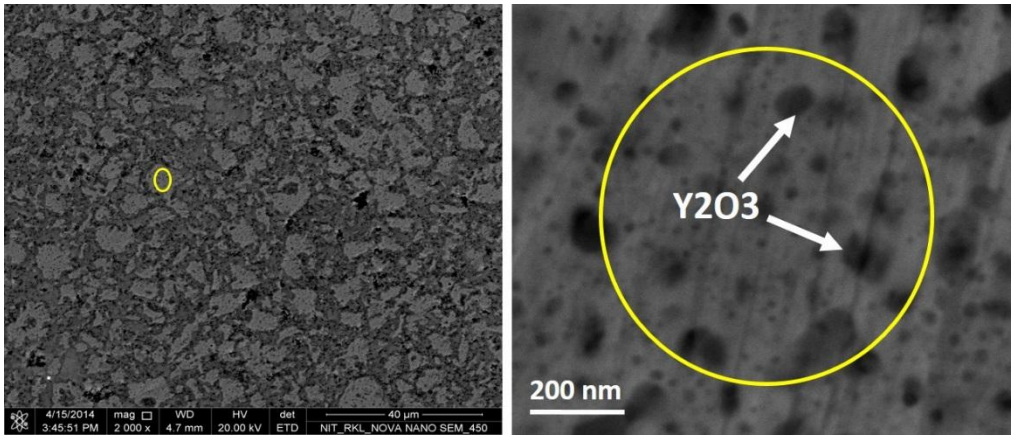

Fig. 4.10: FESEM images of alloy B at different magnifications:
(a) 2500x and (b) 50 000x

The morphology of austenitic and ferritic grains in sintered product of alloy B is revealed by SEM investigation in Fig. 4.10. As discussed earlier bright and dark phases represent Cr-rich (ferrite phase) and Ni-rich (austenite phase) respectively. Correlating the FESEM image C (taken at higher magnification of 50000X) in Fig. 4.10 and EDS mapping of element yttium, Fig. 4.11, (yttrium exists as yttria in the alloy), fine Y_2O_3 particles dispersed in the alloy matrix were identified. The presence of Yttrium and oxygen elements in the EDS pattern of sintered pellet of alloy B (fig. 4.8 b), which was also validated by XRD analysis results stand as further evidence for the existence of Y_2O_3

particles in the alloy. The improvement in the hardness of the steel can be attributed to the distribution of Y_2O_3particles in its matrix (discussed in section 4.8).

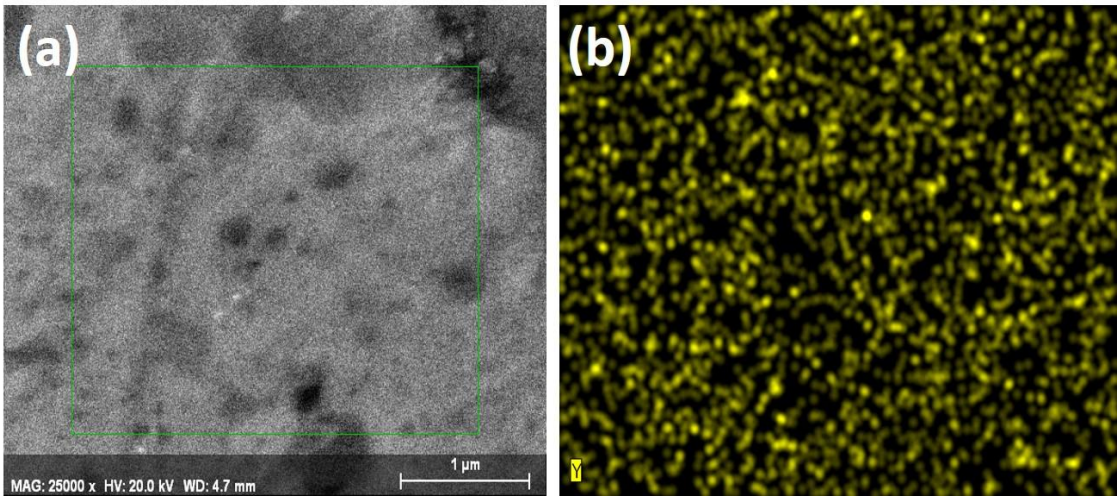

Fig. 4.11: (a-b): EDS element map of Y_2O_3 in alloy B sintered at 1150°C.

4.7.3 Microstructural characterization of alloy C

Similar kind of microstructural features were observed (Fig. 4.12) in the case of alloy C (1 wt. % TiO_2). Dark areas were identified as austenitic regions and bright areas as ferritic regions. The difference being that the alloy B contains Y_2O_3 particle dispersion and alloy C contains dispersion of TiO_2 particles (Fig. 4.13).

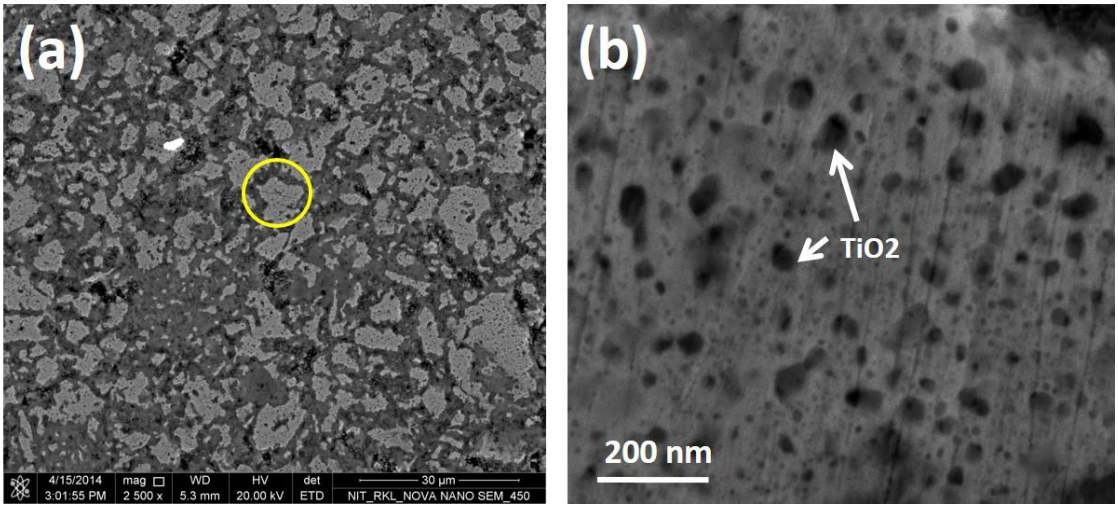

Fig. 4.12: FESEM images of alloy C showing TiO_2 at different magnifications:
(a) 2500x and (b) 50 000x

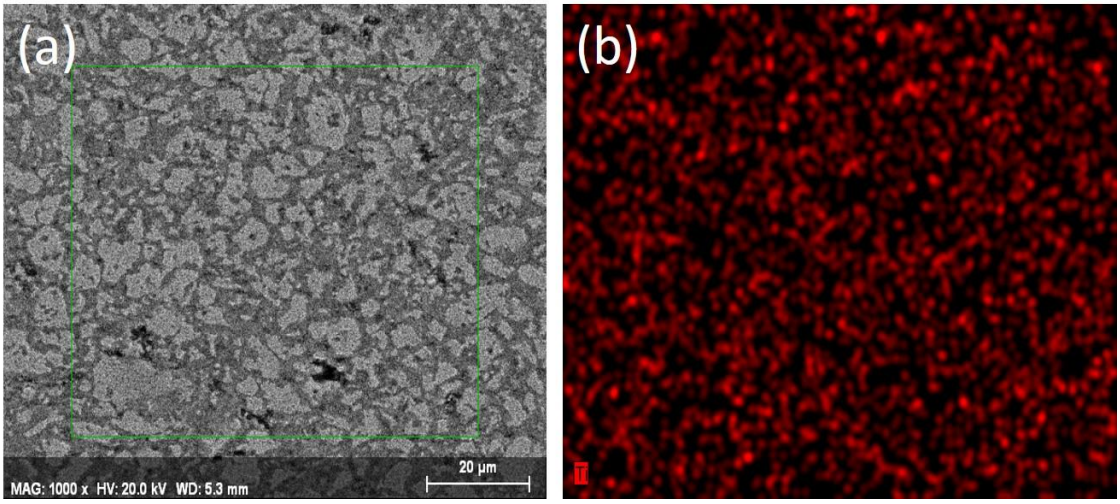

Fig. 4.13 (a-b): EDS Element map of TiO_2 in alloy C sintered at 1150°C.

4.8 Density of consolidated products

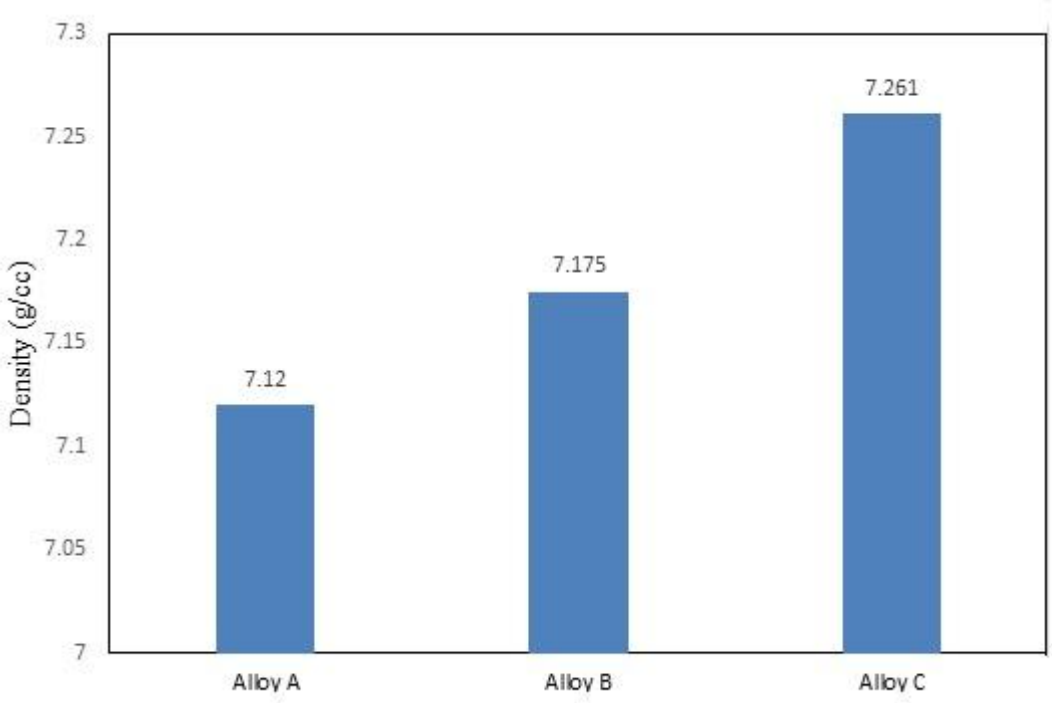

Fig. 4.14: Comparison plot of density for the sintered products

Fig. 4.14 shows the density plot of all the alloys sintered at 1150°C. It reveals that the density of alloy C is higher than to that of alloy A and alloy B. This indicates the porosity of alloy C is 1.07-1.73% lower than that of alloy A and alloy B which is shown in Table 4.5.

Table 4.5: Summary of density/porosity of the sintered products

Alloy	Density (g/cc)	Porosity (%)
Alloy A	7.12	11.22
Alloy B	7.175	10.56
Alloy C	7.261	9.49

4.9 Mechanical properties of sintered products

Fig. 4.15 shows the variation of hardness of the consolidated alloys (alloy A, alloy B and alloy C) which are measured by using Vickers micro-hardness testing machine. Among all the consolidated alloys, alloy C is having more hardness value than that of alloy B and alloy A. This is due to higher densification of alloy C as compared to that of alloy B and alloy A (Fig. 4.15). On the other hand, enhancement of hardness of alloy C is attributed to higher modulus of elasticity of TiO_2 than that of Y_2O_3.

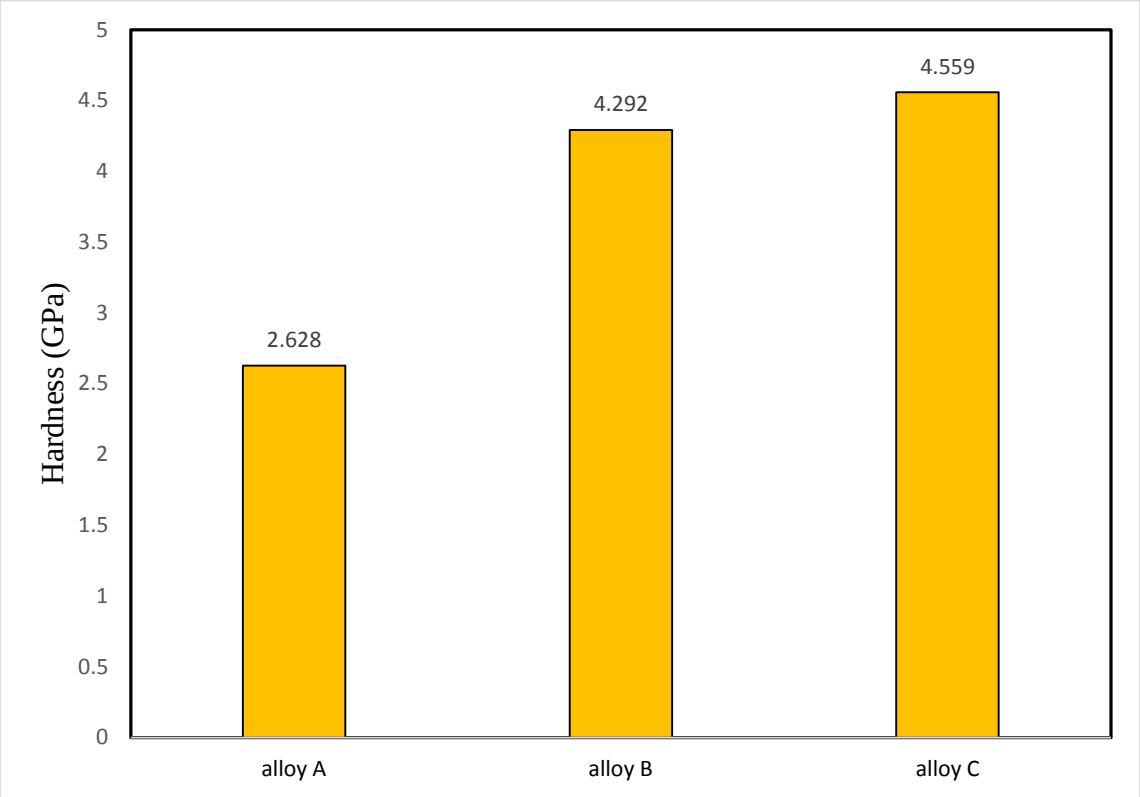

Fig. 4.15: Variation of hardness plot of the consolidated alloys

Improvement of the hardness in the present alloys may be attributed to reduction of grain size by mechanical alloying, which directly follow the Hall–Petch equation [32]. The hard second phase particles or dispersoids in the soft-austenitic matrix which hindered the

dislocation motion hence leads to the enhancement of the hardness of the current alloys. In the present study, improvement of hardness of current alloys followed by the dispersion strengthening mechanism as the uniform distribution of nano-TiO_2/Y_2O_3 into the austenitic matrix. This may be concluding that the solid solution strengthening, refinement of grain size, and dispersion strengthening affecting the increase in hardness of the alloys.

4.10 Wear behaviour study of sintered alloys

Fig. 4.16 shows the plot for the variation of wear depth (μm) vs. time (s) of alloy A, alloy B, and alloy C. It is evident from the plot the maximum wear depth value of alloy C is the least among the three alloys. This result suggests the superior wear resistance of TiO_2 dispersed alloy C over Y_2O_3 dispersed alloy B. While the maximum wear depth values of both alloy A and alloy B were observed to be lower than that of alloy A, indicating the improvement in wear resistance behaviour by oxide dispersion(Y_2O_3/TiO_2) in general.

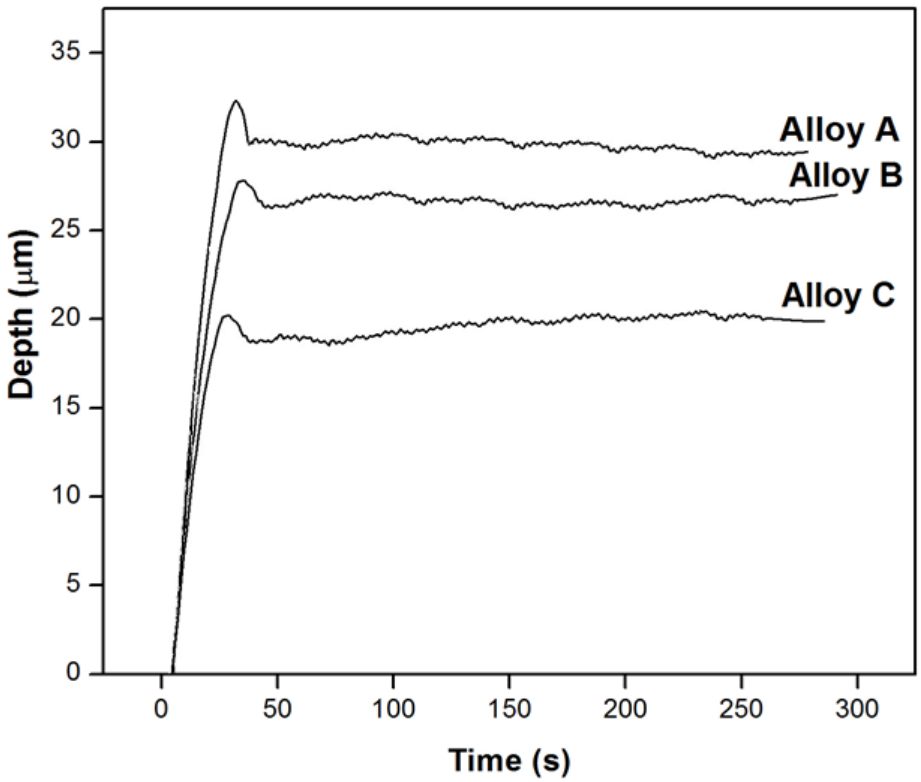

Fig. 4.16: Variation of wear depth vs. time of the sintered products

Figs. 4.17(a-b) show the wear tracks develop during wear testing using 5N load for 5 minutes. It indicates that the degree of loss appears to be a strong indication of localized plastic deformation during wear testing. Examination of the optical images

(Fig. 4.17) point out that the presence of micro-cracks are on the wear tested surface of the alloy sintered at 1150°C.

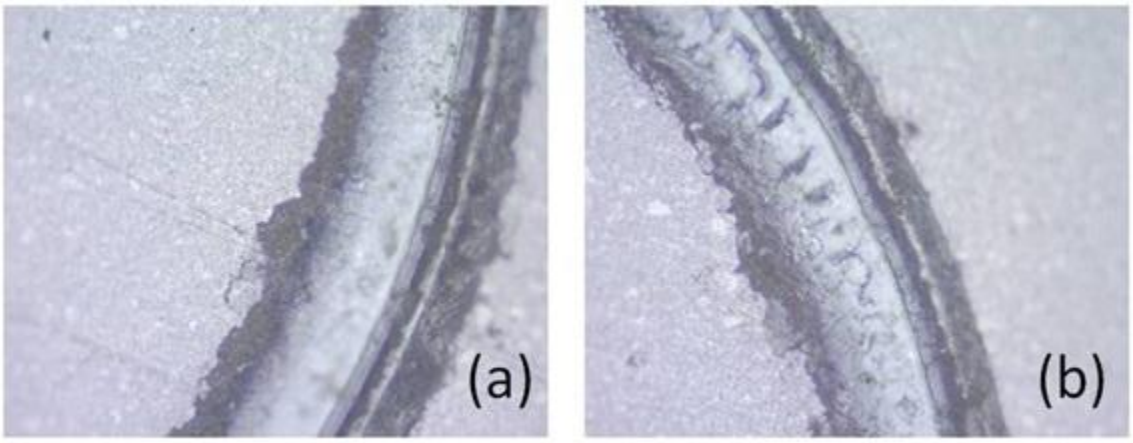

Fig. 4.17 Optical microscope images of wear track.

5. Summary and conclusions

In the present study, a comprehensive effort has been arranged to develop 1.0 wt% nano-Y_2O_3 or TiO_2 dispersed 304L austenitic alloys by mechanical alloying and subsequent consolidation by conventional sintering at 1150° C for 1.0 hour in argon atmosphere. Through close analysis of the results in terms of synthesis and characterization, sintering, density, hardness, and wear resistant property in three set of alloys, a new perceptive on structure-property correlation has distended about nano-oxide dispersed ODS 304L austenitic alloys. The summary and conclusions of the current investigations are primed as follows:

- Mechanical alloying is a novel technique for the synthesis of nano-Y_2O_3 and nano-TiO_2 dispersed ODS 304L austenitic alloys.
- XRD analysis of the milled alloy powder shows that Cr and Ni peaks are completely dissolved in Fe matrix in course of high-energy ball milling for 0-1h. The interesting phenomenon is that the new ferrite peak α and austenitic peak γ have been observed after 1 h of milling, and after 40 h of milling only austenitic peak γ is present.
- Reduction in crystallite size of the parent matrix phase (γ phase) to 210-20 nm with increase of milling time is observed.
- Particle size analysis of different stages of milled powders show the reduction of apparent particle size to51µm to 15µm with increase of milling time. The similar kind of trends has been found by SEM analysis that the average particles size in range of 55µm to 7µm with increase in milling time.
- Presence of the nanometric (20-35 nm) dispersed phases (nano-Y_2O_3or nano- TiO_2) in 304L austenitic matrix are confirmed by FESEM analysis.
- Alloy C (nano- TiO_2 dispersion) consistently records superior property in terms of density, hardness and wear resistant as compared to that of alloy A and alloy B.

Therefore, by evaluation of the above mentioned conclusions recommend that mechanical alloying followed by conventional sintering with nano-oxide dispersed matrix offering attractive mechanical properties.

Reference

[1] Rahul Unnikrishnan, K S N Satish Idury, T P Ismail, Alok Bhadauria, S K Shekhawat, Rajesh K Khatirkar, Sanjay G Sapate, "Effect of heat input on the microstructure, residual stresses and corrosion resistance of 304L austenitic stainless steel weldments,"*Materials Characterization*, 2014, v. 93, pp. 10-23.

[2] Laurent De Baglion, José Mendez, "Low cycle fatigue behaviour of a type 304L austenitic stainless steel in air or in vacuum, at 20 °C or at 300 °C: Relative effect of strain rate and environment," *Procedia Engineering*,2010, v. 2, pp. 2171-2179.

[3] Hiroshi Oka, Masashi Watanabe, Somei Ohnuki, Naoyuki Hashimoto, Shinichiro Yamashita, Satoshi Ohtsuka, "Effects of milling process and alloying additions on oxide particle dispersion in austenitic stainless steel," *Nuclear Materials*, 2014, v. 447, pp. 248-253.

[4] I S Kim, J D Hunn, N Hashimoto, D L Larson, P J Maziasz, K Miyahara, E H Lee, "Defect and void evolution in oxide dispersion strengthened ferritic steels under 3.2 MeV Fe^{+} ion irradiation with simultaneous helium injection," *Nuclear Materials*, 2000, v. 280, pp. 264-274.

[5] A Alamo, V Lambard, X Averty, M H Mathon, "Assessment of ODS-14%Cr ferritic alloy for high temperature applications," *Nuclear Materials*, 2004, v. 329-333, pp. 333-337.

[6] K L Murty, I Charit, "Structural materials for Gen-IV nuclear reactors: Challenges and opportunities," *Nuclear Materials*, 2008, v. 383, pp. 189-195.

[7] N Akasaka, S Yamashita, T Yoshitake, S Ukai, A Kimura, "Microstructural changes of neutron irradiated ODS ferritic and martensitic steels," *Nuclear Materials*, 2004, v. 329-333, pp. 1053-1056.

[8] Shigeharu Ukai, Masayuki Fujiwara, "Perspective of ODS alloys application in nuclear environments," *Nuclear Materials*, 2002, v. 307–311, pp. 749-757.

[9] M K Miller, E A Kenik, K F Russell, L Heatherly, D T Hoelzer, P J Maziasz, "Atom probe tomography of nanoscale particles in ODS ferritic alloys," *Materials Science and Engineering*, 2003, v. 353, pp. 140-145.

[10] Vijendra Singh, "Physical Metallurgy," Standard Publishers Distributors, 2005.

[11] Sidney H Avner, "Introduction to physical Metallurgy," McGraw Hill Education (India) Private Limited, New Delhi, 2013

[12] Setsuo Takaki, Kazuhiro Fukunaga, Junaidi Syarif, Toshihiro Tsuchiyama, "Effect of Grain Refinement on Thermal Stability of Metastable Austenitic Steel," *Materials Transactions*, 2004, v. 45, pp. 2245-2251.

[13] R C Benn, P K Mirchandani, "Dispersion strengthening by mechanical alloying New Materials by Mechanical Alloying Techniques," Artz E, Schultz L:editors, DGM, 1988.

[14] J Rosler, and E Artz, "A new model-based euation for dispersion strengthened materials," *Acta Metallurgica et Materialia*, 1990, v.38, pp.671-683.

[15] J W Martin, “Micromechanisms in particle-hardened alloys,” Cambridge University Press, London, 1980.

[16] R S Herrick, J R Weertman, R Petkovic-Luton, M J Luton, “Dislocation/particle interactions in an oxide dispersion strengthened alloy,” *Scripta Metallurgica*, 1988, v. 22, pp. 1879-1884.

[17] B A Wilcox, A H Clauer, “The role of grain size and shape in strengthening of dispersion hardened nickel alloys,” *Acta Metallurgica*, 1972, v. 20, pp. 743-749.

[18] J H Schneibel, M Heilmaier, W Blum, G Hasemann, T Shanmugasundaram, “Temperature dependence of the strength of fine- and ultrafine-grained materials,” *Acta Materialia*, 2011, v. 59, pp. 1300–1308.

[19] M F Ashby, D R H Jones, “Engineering Materials: An introduction to their properties and applications,” Butterworth Heinemann, 1980.

[20] J K Tien, S Purushothaman, “The metallurgy of high temperature alloys, in Proceedings: Propeties of high temperature alloys-with emphasis on environmental effects,” Foroulis Z A, Pettit F S, eds., The Electrochemical Society, Princeton-NJ publications, v. 77-81, pp. 3, 1976.

[21] Ansell, G S, (1966), in Metallurgical Society conferences on oxide dispersion strengthening, edited by Ansell, G S, T D Cooper and Lenel, F V, (Gordon and Breach, New York, 1966) pp. 61

[22] Gregory, E and Goetzel, C G, “High-temperature properties of nickel-alloy powder extrusions containing nonmetallic dispersions,” *Transaction Metallurgical Society* AIME, 1958, v. 212, pp. 868-874.

[23] K L Murty, I Charit, “Structural materials for Gen-IV nuclear reactors: Challenges and opportunities,” *Nuclear Materials*, 2008, v. 383, pp. 189-195.

[24] Man Wang, Zhangjian Zhou, Hongying Sun, Helong Hu, Shaofu Li, “Microstructural observation and tensile properties of ODS-304 austenitic steel,” *Materials Science & Engineering*, 2013, v. 559, pp. 287–292.

[25] Tae Kyu Kim, Chang Soo Bae, Do Hyang Kim, Jinsung Jang, Sung Ho Kim, Chan Bock Lee, Dohee Hahn, “Micro structural Observation and tensile Isotropy of an ODS steel,” *Nuclear Engineering and Technology*, 2008, v. 40, pp. 305-310.

[26] José M Torralba, Luz Fuentes-Pacheco, Nerea García-Rodríguez, Mónica Campos, “Development of high performance powder metallurgy steels by high energy milling,”*Advanced Powder Technology*, 2013, v. 24, pp. 813-817.

[27] A Le Pécheur, F Curtit, M Clavel, J M Stephan, C Rey, Ph Bompard, “Thermo-mechanical FE model with memory effect for 304L austenitic stainless steel presenting microstructure gradient,” *International Journal of Fatigue*, 2012, v. 45, pp. 106-115.

[28] Hiroshi Oka, Masashi Watanabe, Naoyuki Hashimoto, Somei Ohnuki, Shinichiro Yamashita, Satoshi Ohtsuka, “Morphology of oxide particles in ODS austenitic stainless steel,” *Nuclear Materials*, 2013, v. 442, pp. S164-S168.

[29] Zhangjian Zhou, Shuo Yang, Wanhua Chen, Lu Liao, Yingli Xu, "Processing and characterization of a hipped oxide dispersion strengthened austenitic steel," *Nuclear Materials*, 2012, v. 428, pp. 31-34.

[30] P Susila, D Sturm, M Heilmaier, B S Murty, V Subramanya Sarma, "Effect of yttria particle size on the microstructure and compression creep properties of nanostructured oxide dispersion strengthened ferritic (Fe–12Cr–2W–0.5Y_2O_3) alloy," *Materials Science and Engineering*, 2011, v. 528, pp. 4579-4584.

[31] A Alamo, V Lambard, X Averty, M H Mathon, "Assessment of ODS-14%Cr ferritic alloy for high temperature applications," *Nuclear Materials*, 2004, v. 329-333, pp. 333-337.

[32] C Suryanarayana, "Mechanical alloying and milling," *Progress in Materials Science*, 2001, v. 46, pp. 1–184.

[33] A Bellosi, F Montverde, S Botti, S Martelli. Mater Sci Forum 1997;235-238:255-60.

[34] K Okada, S Kikuchi, T Ban, N Otsuka, *Materials Science Letters*, 1992, v. 11, pp. 862-864

[35] B P Dolgin , M A Vanek, T McGory , D J Ham, "Mechanical alloying of Ni, CO, and Fe with Ti. Formation of an amorphous phase," *Non-Cryst Solids*, 1986, v. 9, pp.87-281.

[36] J S Benjamin, "MECHANICAL ALLOYING," *Scientific American*, 234-, 5, 40, (1976)

[37] J S Bejamin, T E Voilin, "The Mechanism of mechanical alloying," *Material Transaction*, 1974, pp. 5:1929-1934.

[38] P S Gilman, J S Benjamin, "Mechanical alloying," *Annual Review of Materials Science*, 1983, v. 13, pp. 279-300.

[39] J.S. Benjamin, "Dispersion strengthened superalloys by mechanical alloying," *Metallurgical Transactions*, 1970, v. 1 (10), pp. 2943-2951.

[40] P Y Lee, C C Koch, *Appl Phys Lett*, 1987, v. 50, pp. 1578-80.

[41] R M Davis, CC Koch, "Mechanical alloying of brittle components: silicon and germanium," *Scripta Metall*, 1987, v. 21, p. 305-10.

[42] R M Davis, B T McDermott, C C Koch, "Mechanical Alloying of Brittile Materials," *Metall Trans*, 1988, v. A19, p. 2867-2874.

[43] P Y LEE, C C KOCH, "The formation and thermal stability of amorphous Ni-Nb alloy powder synthesized by mechanical alloying," *Non-Crystalline Solids*, 1987, v. 94, pp. 88-100.

[44] C C Harris, "On the Role of Energy in Comminution," *Trans Soc Min Engrs*, 1967, v. 238, p. 17.

[45] G S Upadhyaya, "Powder Metallurgy Technology," Cambridge International Science Publishing, England, 2002.

[46] P C Angelo, R Subramanian, "Powder Metallurgy: Science, Technology and Applications," ISNB-978-81-203-3281-2

[47] Shigeyuki Somiya, Fritz Aldinger, Richard M. Spriggs, Kenji Uchino, Kunihito Koumoto, Masayuki Kaneno, Handbook of Advanced Ceramics: Materials, Applications, Processing and Properties, v. 2, Academic Press, 2003.

[48] B W Mott, "Micro indentation Hardness Testing," Butterworths Scientific Publication, London (1956)

[49] D Tabor, "The Hardness of Metals," Clarendon Press, Oxford (1951).

[50] R Jenkins, R L Snyder, "Introduction to X-Ray Powder Diffractometry," JWiley & Sons Inc., New York, 1996.

[51] R Shashanka, D Chaira, "Phase transformation and microstructure study of nano-structured austenitic and ferritic stainless steel powders prepared by planetary milling," *Powder Technology*, 2014, v. 259, pp. 125-136.